Published in final edited form as:
J Mol Biol. 2010 January 29; 395(4): 815. doi:10.1016/j.jmb.2009.10.029.

Mechanical coupling in myosin V: a simulation study

Victor Ovchinnikov[a,1], **Bernhardt L. Trout**[a], and **Martin Karplus**[b,2]

Victor Ovchinnikov: ovchinnv@MIT.edu; Bernhardt L. Trout: trout@MIT.edu; Martin Karplus: marci@tammy.harvard.edu

[a] Department of Chemical Engineering, Massachusetts Institute of Technology, Cambridge, MA, 02139

[b] Laboratoire de Chimie Biophysique, ISIS, Université de Strasbourg, 67000 Strasbourg, France

Abstract

Myosin motor function depends on the interaction between different domains that transmit information from one part of the molecule to another. The inter-domain coupling in myosin V is studied with Restrained Targeted Molecular Dynamics (RTMD) using an all-atom representation in explicit solvent. To elucidate the origin of the conformational change due to the binding of ATP, targeting forces are applied to small sets of atoms (the forcing sets, FS) in the direction of their displacement from the rigor conformation, which has a closed actin-binding cleft, to the post-rigor conformation, in which the cleft is open. The 'minimal' FS that results in extensive structural changes in the overall myosin conformation is comprised of the ATP, Switch 1, and the nearby HF, HG and HH helices. Addition of switch 2 to the forcing set is required to achieve a complete opening of the actin-binding cleft. The RTMD simulations reveal the mechanical coupling pathways between (i) the nucleotide-binding pocket (NBP) and the actin-binding cleft, (ii) the NBP and the converter, and (iii) the actin-binding cleft and the converter. Closing of the NBP due to ATP binding is tightly coupled to the opening of the cleft, and leads to the rupture of a key hydrogen bond (F441N/A684O) between switch 2 and the SH1 helix. The actin-binding cleft may mediate the rupture of this bond *via* a connection between the HW helix, the Relay helix, and Switch 2. The findings are consistent with experimental studies and a recent normal mode analysis. The present method is expected to be useful more generally in studies of inter-domain coupling in proteins.

Keywords

myosin V; conformational change; subdomain coupling; targeted molecular dynamics; proteins

1. Introduction

Unconventional myosin V is a versatile cellular transporter, capable of dimerization and motion along actin filaments. Each myosin V molecule in a dimer possesses a globular motor domain to which a long lever arm is attached. The lever arm precedes a coiled-coil dimerization region, and a globular cargo-binding domain. Myosin V dimers have been shown to "walk" along actin filaments in a hand-over-hand fashion, with one motor domain bound tightly to actin, while

Correspondence to: Martin Karplus, marci@tammy.harvard.edu.

[1]Present address: Department of Chemistry and Chemical Biology, Harvard University, Cambridge, MA, 02138
[2]Alternative address: Department of Chemistry and Chemical Biology, Harvard University, Cambridge, MA, 02138

the other steps forward in search of its next binding site.[1] Walking with steps of 36 nm on the average,[2] a myosin V dimer is capable of transporting cellular cargo along actin filaments for distances of up to 1 μm before dissociation.[1]

The swinging lever arm hypothesis[3] is the most widely accepted model of myosin V function. This model describes a cycle in which the release of ATP hydrolysis products, ADP and the P_i ion, are translated into a large mechanical motion of a converter subdomain. This motion is further amplified through the long elastic lever arm, and accounts for most of the stepping. A simplified depiction of the myosin V cycle is shown in Fig. 1. The cycle is comprised of actin-bound and free-myosin states. The former are required for force generation, and the latter, for ATP hydrolysis. The cycle begins with the free (*i.e.* not bound to actin) myosin motor with ATP in the nucleotide pocket (post-rigor state). ATP hydrolysis occurs spontaneously, but product (ADP and phosphate [P_i]) release is inhibited until the motor binds to actin in the pre-powerstroke state. The release of P_i from the actin-bound form is thought to initiate the power stroke. The motor undergoes additional conformational changes that result in a strong actin-binding interface and leads to the release of ADP. The resulting strong actin-bound nucleotide-free (rigor) state, which is important for processive motion, is followed by the binding of a new ATP molecule to the actomyosin complex. Dissociation of myosin from actin follows, and the motor returns to the post-rigor state, in preparation for the next cycle.

Three high-resolution myosin V structures in the absence of actin have been solved: the rigor-like, post-rigor, and a weakly-bound ADP structure,[5] which is very similar to the rigor structure.[6] Currently, no crystal structure of the pre-powerstroke state of myosin V exists. Although myosin V spends most of its time bound to actin,[7] the only available structures of the actomyosin complex are based on relatively low-resolution cryo-electron microscopy.[8, 4, 9] In the rigor-like structure, the actin-binding cleft is 'closed,' as appears to be required for strong binding to actin.[6] This structure can be fit into the cryo-electron microscopy density of the actomyosin complex without distortion.[4] It has been shown that the binding of myosin V to actin in the absence of ATP is diffusion-limited. This finding supports the hypothesis that the rigor-like structure binds to actin without significant structural rearrangements.[6] Henceforth, we refer to this structure simply as the 'rigor' (R) structure. Other hallmarks of the rigor state include an open and empty nucleotide-binding pocket (NBP) and a converter in the post-powerstroke conformation, which is coupled to the rest of the motor more tightly than in the other structures.[6, 10] The post-rigor (PR) structure of myosin V evolves from the rigor state upon the binding of ATP and dissociation from actin. Its features are an open actin-binding cleft, a partially closed ATP binding pocket, and a converter conformation that is more loosely coupled to the rest of the motor domain than in the rigor structure.

The rigor and post-rigor myosin V structures, with key domains in different conformations, represent an excellent system for probing by simulation the mechanical coupling between the subdomains of myosin V. In the first study of the transition between the rigor and post-rigor structures,[10] a superposition of normal modes was used to obtain insights into the interdomain coupling involved in the rigor to post-rigor transition. It was suggested that the trigger for the transition is the interaction between switch 1 and the P-loop, which is stabilized by ATP in the post-rigor state. A limitation of the normal mode superposition model (NMSM) is that it does not provide direct evidence for the sequence of events in the transition. Thus, it is important to evaluate the conclusions obtained from NMSM by an independent method. In the current investigation, we use Targeted Molecular Dynamics with an external restraining potential (RTMD), instead of holonomic constraints[11] to demonstrate the origin of the coupling between three regions in the myosin V motor domain: (i) the actin-binding cleft, (ii) the nucleotide-binding pocket, and (iii) the converter. Starting from either the rigor or the post-rigor structure of the myosin V motor, we apply targeting forces to a small part of this structure and observe the response in other (unforced) regions of the structure. The targeting forces are derived from

a potential based on the root-mean-square distance (RMSD) of the selected elements between their positions in the simulation structure and in the target crystal structure, and steer the chosen elements toward their 'target' conformation. The goal of the study is to identify key structural elements that are essential for transitions between the rigor and post-rigor structures, and the pathway(s) by which these transitions are likely to occur.

We find that applying targeting forces to certain elements in the vicinity of the nucleotide-binding pocket (defined by residue segments 162–169 [P-loop], 207–219 [Switch 1], and 437–448 [Switch 2][5]) of the rigor structure leads to two major rearrangements in the motor domain: (i) opening of the actin-binding cleft and (ii) uncoupling of the converter from the rest of the motor. In addition, applying targeting forces to the same elements in the post-rigor structure leads to partial closure of the cleft. The results provide an atomic-level description of the communication pathways between the three regions of the myosin V motor, and yield insights into the likely transition pathway between the rigor and post-rigor states. The results are consistent with predictions based on kinetic and crystallographic studies of myosin V, as well as the all-atom block normal mode superposition model of Cecchini et al.[10] Although numerous computational studies of Myosin II at the atomic level have been published[12, 13, 14]), to our knowledge, this is the first all-atom RTMD investigation of Myosin V.

2. Results

This section is organized as follows. In section §2.1 we describe the results of equilibrium NVE simulations of the R and PR structures of the myosin V motor. The NVE simulations were used to investigate the stability of the simulation structures, to provide a measure of the flexibilities of the myosin V subdomains, and to determine order parameters for the RTMD simulations, as described in §2.2. Results of the RTMD simulations are described in §2.3. Three different forcing sets (FS) are considered, in the order of increasing FS size, to study the coupling between various parts of the structures and to identify the subdomains essential for the rigor R → PR transition.

2.1. NVE simulations

Two 18ns equilibrium NVE simulations were performed in this study. They are summarized in Tab. 1. Both conformers were stable over the simulation time, with backbone RMSD between the final structure from the simulations and the corresponding crystal structures of the motor domain around 1.7Å (this value may be compared with the RMSD value of 3.5Å between the motor domains in the two crystal structures; at the end of the NVE simulations, the RMSD between the two motor domains increases slightly to 3.9Å). The root-mean-square fluctuations (RMSF) of the individual residue positions relative to the corresponding average positions computed from the simulations are shown in Fig. 2. Comparison with the RMSF computed from temperature factors in the PR PDB file indicates that the simulation structures reflect the properties of the experimental structures. The correlation coefficient between the PR simulation data and the corresponding PDB data is 0.75. We found that the B-factors in the PDB file for the R structure (not shown) were larger than those in the PR file. Despite the differences in magnitudes, the B-factors in the two datasets are correlated with a correlation coefficient of 0.76. The calculated fluctuations for the rigor and post-rigor conformers are highly correlated, with a correlation coefficient of 0.89. In particular, residues that comprise Switch 1 have low RMSF values in both cases, indicating that Switch 1 is not flexible even in the absence of ATP. The RMSF of residues in the Relay helix increases in the C-terminal direction (res. 449–481). This is probably due to the fact that the C-terminus of the Relay helix is coupled to the converter, which undergoes large fluctuations.

The fact that nearly all converter residues have higher fluctuations in the PR state suggests that the post-rigor converter is coupled less strongly to the motor domain. This is required for the

recovery stroke, which follows ATP binding and hydrolysis in the myosin cycle, and repositions the converter and the lever arm in the pre-powerstroke conformation. The heavy-atom RMSD of the converter domain in the simulation structures from the corresponding starting crystal structure calculated after best-fit alignment using only the motor domain (converter not included), were ≃ 2.0Å and ≃ 2.6Å for R and PR simulations, respectively, consistent with the present interpretation of the RMSF plots.

2.2. Order parameters

To characterize the differences between crystal and simulation structures, it is convenient to define a set of order parameters (OP) that describe the conformations of the various subdomains. The OP are chosen such that their values corresponding to the two states are significantly different. Such OP are also convenient to describe the progression of the structural changes in the RTMD simulations. Mean OP values obtained from equilibrium simulations can be compared to the corresponding time-series from RTMD simulations to assess the significance of the structural changes taking place in the RTMD. For example, the distance between centers of mass (COM) of residues 516 and 347 of the HC are representative of the extent of closure of the actin-binding cleft. It will be shown that as the cleft opens in the RTMD simulations, this distance increases, yet fluctuates around the corresponding mean values in the equilibrium NVE simulations.

The OP used in this study are listed in Tab. 2 and illustrated in Fig. 3. Subdomain definitions are provided in Tab. 3. and the corresponding subdomains are shown in Fig. 4. The entries in Tab. 2 are grouped into four categories.

- **a.** OP 1–5 (Fig. 3a) correspond to hydrogen bonds in the actin-binding cleft that rupture when the cleft opens.
- **b.** OP 6–9 (Fig. 3b) correspond to four inter-residue distances that quantify the degree of cleft opening.[24] OP 9 corresponds to the COM distance between R213 in Switch 1 and F444 in Switch 2 and, therefore, is also an indicator of the Switch 2 position relative to the NBP.
- **c.** OP 10–12 (Fig. 3c) quantify the orientation of Switch 2, the Relay helix, and the SH1 helix. These OP serve to describe a communication pathway between the actin-binding cleft and the converter domain that appears to be modulated by the NBP, and involves a key hydrogen bond between F441 (Switch 2) and A684 (SH1 helix).
- **d.** OP 13–14 (Fig. 3d) describe the relative orientation of helices HF, HG, and HH. Since the HF helix comprises the orientation set, and the HG/HH helices are part of the forcing set in four RTMD simulations presented, these two OP describe the progress of the conformational changes that are forced (i.e. these change are not due to coupled interactions involving freely-moving atoms).

Tab. 2 provides mean OP values obtained from the equilibrium NVE simulations. A comparison of OP evolution in equilibrium NVE and nonequilibrium RTMD simulations is made in §2. The values of all OP computed at the end of each simulation are provided in the Supplementary Materials.

2.3. RTMD simulations

The purpose of the RTMD simulations was to determine whether enforcing conformational rearrangements of parts of the molecule in the vicinity of the NBP would lead to changes in other parts of the motor domain. Tab. 4 provides a summary of the RTMD simulations performed in this study. A typical RTMD simulation (*e.g.* RTMD simulation 2 in Tab. 4 was performed as follows. In the equilibrated crystal structure of the rigor-ATP conformer, the

backbone atoms of the HF helix were harmonically restrained to their positions in space. The HF helix also comprised the set of RTMD orientation atoms, although this is not a requirement. Forces derived from the RTMD potential were applied to the forcing set. The target RMSD, i.e. δ in Eq. (1), was reduced uniformly from the initial RMSD value, denoted by δ_0, to 0.1Å over 0.7ns; i.e. δ was reduced by ≃0.00002Å per simulation timestep (2fs). With δ fixed at 0.1Å, the simulation was continued for another 7.7ns until t=8.4 to allow the simulation structure to equilibrate in the presence of the applied forces. The backbone-atom RMSD of the motor domain between the final RTMD structure and the target structure is an approximate indicator of the extent of the overall conformational change. For simulation 2, this value is 2.16Å (Tab. 4), compared with the initial RMSD value of 3.5Å between the rigor and post-rigor structures.

Simulation 2e in Tab. 4, is a continuation of simulation 2 in which the RTMD force constant was uniformly reduced to zero starting at t=8.4 until t=9.4, and the simulation was continued for 7.4 ns in the absence of any restraints. The purpose of this simulation was to see the extent to which the structural changes in the motor domain observed in simulation 2 would be retained in the absence of the RTMD forces.

We begin the discussion with the RTMD simulations that correspond to the R→PR transition of the forcing set. Simulations 1, 2, and 3, which are performed using FS of increasing size, are discussed in order. The primary focus is on simulation 2 because it captures most of the essential features of the R→PR transition of the motor domain. By contrast, in simulation 1, the extent of the overall conformational change resulting from the RTMD forces is significantly less. In simulation 3, the conformational change is more complete. However, the forcing set is expanded to include 101 additional atoms (353 atoms vs. 252 atoms in simulation 2). Simulation 2e, in which the RTMD forces were gradually turned off, and Simulation 4, which corresponds to the PR→R transition of the forcing set used in simulation 2, are discussed in the Supplementary Materials. The evolution of the OP in simulations 2 and 3 is discussed in this section, and shown in Fig. 6. OP evolution corresponding to the other simulations is summarized in the Supplementary Materials.

Simulation 1—The forcing set used in simulation 1 involves only the residues of the NBP along with the MgATP, and is a natural choice for enforcing NBP closure. However, although the position of NBP/MgATP at the end of the simulation is consistent with the PR conformation, only modest opening of the actin-binding cleft is achieved. Examination of the RTMD trajectory revealed that the HG and HH helices, which are adjacent to switch 1, were not positioned as in the target (PR) structure (Fig. 5). The green arrow in the figure points in the direction of displacement of helices HG/HH relative to helix HF determined from the two crystal structures. Most of the displacement occurs along the axis of the HG/HH helices, such that the minimum distance between the backbones of the HG/HH and HF helices remains approximately the same. The red arrow in Fig. 5 corresponds to additional rotational motion of helices HG/HH observed in the RTMD simulation. The final simulation position of the HG/HH helices is inconsistent with the PR structure; in particular the distance between helices HG/HH and helix HF is increased. The inconsistent positioning appears to result from steric clashes between the sidechains of helices HF and HG/HH, involving residues K174, L197, R178, and E193. They arise when Switch 1 is pulled towards the P-loop by the RTMD forces to close the NBP. As a result, the HG/HH helices are farther from helix HF than in the target conformation (Fig. 5).

Although the binding of MgATP to the NBP initiates the R→PR conformational change, applying RTMD forces to the NPB and MgATP alone is not only insufficient to open the cleft, but also leads to some distortion of the simulation structure.

This is not surprising because conformational changes in the FS are induced on the subnanosecond timescale (Tab. 4), compared to the millisecond timescale of ATP binding measured in experiments,[7] and the micro- to millisecond timescales generally required for large conformational changes in proteins. Thus, closing of the NBP occurs much too rapidly in the simulation, introducing RTMD forces that are excessively large and giving rise to significant deviations from an equilibrium trajectory. Since it is not possible to reach the experimental time scale in MD simulations of our system because of its large size, an alternative solution is to expand the forcing set (FS), as described next.

Simulation 2—Examination of the trajectory from simulation 1 revealed that the HG/HH helices remained in a similar position relative to the HO helix, indicating that these three helices are coupled. For example, when the PR structure and the final structure from simulation 1 were aligned to minimize the RMSD between the backbone atoms in the HO helix, the RMSD between the backbone atoms in helices HG/HH was 2.2Å although the RMSD between the backbone atoms in the HF helix was 3.4Å. This indicates that the HG/HH helices undergo significantly smaller displacements relative to the HO helix than does the HF helix.

As can be inferred from Fig. 5, the interaction between the HO and HG/HH helices is due primarily to van der Waals forces involving residues I415, F412, L423 in (HO helix), and residues V196, I202, M203, and I206 (HG/HH helices). A hydrogen bond between A422 (backbone oxygen) and K195 (side-chain nitrogen) couples the ends of helices HO and HG. If the coupling is sufficiently strong, motions of the HG/HH helices, even on a short time scale, will cause the HO helix to move as well. Fig. 3 shows that the HO helix forms part the actin-binding cleft, so that its motion will affect the state of the cleft. The fact that the positions of the HO and HG/HH helices appeared to be coupled was not surprising, since these helices all belong to the upper 50kDa domain, which was predicted to move as a quasi-rigid body.[25] This conclusion is supported by recent normal mode calculations.[10] In contrast, the HF helix belongs to the N-term domain, so that significant motion of this helix, relative to helices HG/HH and HO, is not surprising.

Motivated by these observations, we expanded the FS in RTMD simulation 2 to include all heavy atoms of helices HG/HH. MgATP is also included in the FS, as in RTMD simulation 1. The P-loop was included in the FS of simulation 1 to safeguard against possible distortions of the NBP, since significant forces are applied to Switch 1 and MgATP. However, because restraint forces are also applied to the HF helix, which is adjacent in sequence to the P-loop, and thus hinders its movement, and because the difference between the P-loop position in the R and PR structures is small (after superposition on the HF helix, see e.g. Fig. 5, it was removed from the FS of simulation 2. Simulation 2 structures shown below indicate that the P-loop preserves its structure.

This choice of forcing set leads to greater opening of the actin-binding cleft *via* the coupling between the HG and HO helices. It also results in motion of Switch 2 and the Relay helix relative to the SH1 helix, which loosens the coupling between the converter and the rest of the motor.

The observations from the simulation can be grouped into three categories: (1) coupling between the NBP and the actin-binding cleft, (2) coupling between the NBP and the converter, and (3) coupling between the cleft and the converter. These coupling modes are discussed in turn. The evolution of the OP defined in Tab. 2 during simulation 2 is shown in Fig. 6a–e (t=0–8.4). In the figure we also include the OP evolution in simulation 3, which is discussed at the end of this section, and the OP values from the equilibrium (NVE) simulations of the R and PR structures. (Simulation time is quoted in nanoseconds).

Because helices HG/HH are explicitly included in the forcing set, RTMD ensures that their final position corresponds to the post-rigor conformation. OP 13 and 14 in Tab. 2 monitor the relative orientations of the HF and HG/HH helices. Fig. 6e shows that helices HG and HH in the forcing set have moved into their final position by $t = 0.7$. The state of the actin-binding cleft is monitored by OP 6–9, whose evolution in time is shown in Fig. 6b. The figure reveals that at $t = 0.7$ the cleft is still essentially closed: only the far inner part of the cleft (OP 9) has opened appreciably. However, this result is not indicative of coupling between the comformations of the NBP and the cleft, because one of the residues in OP 9, R213, belongs to switch 1, which is included in the forcing set (see Tab. 4) Moreover, Fig. 6l indicates that the values for this OP tend to their PR levels in equilibrium NVE simulations of the R state, while other cleft OP remain consistent with the R state. Significant opening of the far outer cleft occurs at $t \simeq 1.45$ (OP 6), and the cleft opens even more in the following three nanoseconds (Fig. 6b). From this point on ($t \simeq 4.5$), the extent of cleft opening remains the same until the end of the simulation. That the response of the cleft is not instantaneous is not surprising, since it requires the communication of forces along a complex pathway, which we now describe.

As in simulation 1, the relative position of helices HO, HG, and HH remains approximately the same as in the initial, rigor, conformation (this is also in accord with the PR structure). Moreover, the position of the N-terminus of the HO helix is approximately in its final position by $t = 1.0$, which suggests strong coupling, and fast communication, between helices HO and HG/HH (helices HG/HH are in position by $t = 0.7$). This is shown in Fig. 7, in which we overlay the initial, the target, and two simulation structures that correspond to t=1.0 and t=8.4. Repositioning the HG/HH helices into the post-rigor conformation induces a large ‘upward’ movement of the N-terminus of the HO helix.

The subsequent opening of the actin-binding cleft at t=1.45 is accompanied by rearrangements in a tightly-knit pattern of hydrogen bonds that involve residues N398 and K405 in the HO helix, residues K569, D570 in the strut, residue K246 in the upper 50kDa domain, residue Q639 in the HW helix, and residue E566 in the lower 50kDa domain. These rearrangements are illustrated in Fig. 8, which shows the state of the cleft in the initial and final simulation structures. The force on the HO helix due to the displacement of the HG/HH helices imposes a stress on the hydrogen bonds N398[HO]/E566[L50], K405[HO]/D570[strut], and K405 [HO]/D569[strut], K246[U50]/Q639[HW], D570[strut]/Q639[HW]. These bonds correspond to OP 1–5 in Tab. 2. The hydrogen bond N398[HO]/E566[L50] is present only part of the time in the reference equilibrium simulation of the rigor state (Fig. 6f). It is considered intact if the distance between the heavy atoms N389N_{δ} and E566O_{ε} is less than 3.5Å and the donor/ hydrogen/acceptor angle is between 90° and 180°. In the equilibrium MD trajectory, it is intact 42.5% of the time. After $t = 1.4$ in the RTMD trajectory, this bond is intact only 13.5% of the time. Fig. 6a,b indicate that the breaking of the hydrogen bonds K405/D570, K405/D569, and K246/Q639 correlates with the opening of the outer cleft.

The last hydrogen bond, D570/Q639, breaks around $t = 5$ but its rupture does not result in a wider cleft. Rather, it appears to influence the positioning of the Relay, as discussed below. The width of the actin-binding cleft at the end of simulation 2 is still about 3Å less than that in the NVE PR simulation. Further cleft opening appears to require a displacement of switch 2, which does not occur in this simulation. The displacement of switch 2 is forced in RTMD simulation 3, as discussed at the end of this section.

Coureux et al.[6] observed that in the rigor state, the converter is attached to the motor domain more rigidly than in the post-rigor state. RTMD simulation 2 explains the nature of the coupling between the conformations of the NBP and the converter and the role of this coupling in the R→PR transition. OP 11–12 in Tab. 2 (Fig. 3c) are used for this discussion. OP 11 corresponds to a hydrogen bond between the backbone atom A684O in the N-terminus of the SH1 helix

and the backbone atom F441N in Switch 2. This bond is absent in the post-rigor conformation, and is also absent in all other existing crystal structures of myosins. It remains intact during equilibrium MD simulation of the R structure (Fig. 6n), which suggests that it is directly involved in the more rigid attachment of the converter domain in the rigor state. The stronger converter attachment in the rigor state vs. the post-rigor state is consistent with the data in Fig. 2, which show that residues in the converter domain have lower RMSF values during equilibrium MD simulations of the rigor structure.

Fig. 6d shows the evolution of OP 11 during simulation 2 (see Fig. 3c for an illustration of OP 11 and 12). The hydrogen bond is stable until $t = 1.4$, at which time it begins to fluctuate. This time coincides roughly with the breaking of the three hydrogen bonds in the actin-binding cleft discussed above. Approximately three nanoseconds into the simulation, the OP 11 hydrogen bond breaks and the OP value rises to about 5.5Å. The breaking of this hydrogen bond is accompanied by the motion of Switch 2 away from the SH1 helix. The behavior of OP 12, shown in Fig. 6d, indicates that this motion is also coincident with a movement of the Relay helix relative to the SH1 helix. In Fig. 9a we superimpose the initial, final, and target structures from the RTMD simulation 2. By the end of the simulation, the Relay helix has undergone a large displacement relative to the SH1 helix. Breaking of the hydrogen bond F441N/A684O (OP 11) appears to be required for the Relay to “slide” along the SH1 helix because residue F441 belongs to Switch 2, which is connected to the N-terminus of the Relay. The ‘upward’ motion of the of Relay displaces the base of the converter in the direction of the cleft and induces its rotation. Thus, the movement of Switch 1 and the HG/HH helices in simulation 2, consistent with the closing of the NBP, appears to ‘uncouple’ the converter subdomain from the rest of the motor via the rupture of the F441N/A684O hydrogen bond. The importance of this hydrogen bond was also noted in the NMSM model of Cecchini et al. (2008). The interface between the Relay and the SH1 helices involves several hydrophobic residues. It has been proposed that this interface facilitates the relative motion of the two helices.[6]

Fig. 9a shows that the final position of the converter in simulation 2 is still inconsistent with the PR conformation. Correct positioning would require additional motion of the C-terminus of the Relay helix, accompanied by a more extensive converter rotation. Since the interface between the converter and the N-terminal domain of the motor is lined by several nonpolar residues,[6] additional converter motion may be hindered by barriers due to van der Waals interactions. Overcoming such barriers would probably require longer MD simulations.

The final coupling pathway involves the actin-binding cleft and the converter domain. Because switch 2 is an essential element in the corresponding communication pathway, we discuss it in the context of RTMD simulation 3 (below), in which the effect of conformational change in Switch 2 on the rest of the motor domain is considered explicitly.

Simulation 3—In simulation 3, the forcing set of simulation 2 was expanded to include all heavy atoms of Switch 2 to study specifically the influence of its position on the conformational change in the motor domain. Fig. 10b shows that the position of Switch 2 at the end of simulation 3 is much closer to the target PR structure than it is at the end of simulation 2 (Fig. 10a).

Since the FS of simulation 3 contains the FS of simulation 2, we expected to observe all of the events that occur in simulation 2. This is indeed the case, as can be inferred from Fig. 6f–i, which show the rupture of the cleft hydrogen bonds (f), cleft opening (g), straightening of the Relay helix (h), and uncoupling of the converter via the F441/A684 hydrogen bond (i). However, in contrast to the results of simulation 2, Fig. 6g, shows that the actin-binding cleft opens fully by $t \simeq 6$. Thus, complete opening of the cleft involves greater motion of Switch 2 than was observed in simulation 2. In addition, the final simulation values for OP 1–5, which

correspond to hydrogen bonds in the cleft are closer to their values in the PR conformation, consistent with the wider cleft.

The difference between the final position of Switch 2 in simulations 2 and 3 involves a salt bridge between residues R219 in Switch 1 and E442 in Switch 2. In the R structure, this salt bridge is intact, keeping Switch 1 and 2 closer together, while in the PR structure it is broken, and allows a greater distance between Switch 2 and Switch 1 (see Fig. 10).

Thus, RTMD simulation 3, in which the FS of simulation 2 is expanded to include the heavy atoms of switch 2, indicates that proper positioning of the L50 domain relative to the U50 domain, as well as a full opening of the cleft, involves the breaking of the salt bridge between R219[Switch 1] and E442[Switch 2], which occurs when Switch 2 is moved away from Switch 1. Nevertheless, simulation 2 indicates that the "triggering event" for the R→PR transition is just the rearrangement of the NBP due to the binding of ATP (as suggested by Cecchini et al. [10]). Breaking of the hydrogen bonds between R219 and E442, the accompanying motion of Switch 2, and the full opening of the actin-binding cleft, are expected to occur spontaneously after the binding of ATP, albeit on a longer timescale than that in the simulations.

The nature of the coupling between Switch 2 and the cleft can be understood from Fig. 11, in which we have superimposed the R and PR crystal structures. Unlike in the previous figures, the superposition is based on the Relay and SH1 helices to make the the relevant motion of the Relay N-terminus clearer (although the following discussion is also consistent with Fig. 9. In the two crystal structures, the N-terminus of the Relay (F449–K460) has slightly different positions relative to the SH1 helix. The difference is quantified by OP 10, which corresponds to the angle between the axis of the SH1 helix, and the axis of the Relay N-terminus, (see Tab. 2, and in Fig. 3c, In the R structure, OP 10 equals ≃ 40°, compared to ≃ 30° in the PR structure. Fig. 11 shows that forcing Switch 2 from the R to the PR conformation changes the position of the N-terminus (top) of the Relay helix. The Relay then transmits a force to the HW helix via residue F449. As the HW helix is displaced deeper into the actin-binding cleft, it pushes the HR helix farther away from the HO helix, widening the cleft. The coupled motion of the Relay, HW and HR helices is not surprising, since they all belong to the L50 domain, which has been shown to move as a quasi-rigid body[25, 10]).

3. Discussion

Previous experimental and computational studies have proposed that the function of molecular motors of the myosin family can be understood in terms of the coupling between several quasi-rigid subdomains connected by more flexible tethers.[26, 27] In this work, we used a restrained TMD algorithm to test directly the hypothesis of mechanical coupling between three domains of myosin V: the NBP, the actin-binding cleft, and the converter. Specifically, starting with the rigor conformation, we applied forces to a small set of atoms in the vicinity of the NBP to force this set into the conformation consistent with the post-rigor structure. At the same time, we monitored other parts of the motor for structural changes. The choice of the NBP as the forcing set is consistent with the experimental observation that the the R→PR transition is initiated by the binding of ATP to the NBP.[7, 8] Four RTMD simulations were performed in the direction of the R→PR transition, which vary in the composition of the forcing set, and the strength and duration of the applied forces. An additional RTMD simulation was performed in the reverse direction. RTMD simulation 2 was the focus of the analysis, because it involves a (minimal) forcing set that triggers the major features of the transition, and illustrates the essential pathways of inter-domain coupling.

Coureux et al.[6] have shown by soaking MgADP into a crystal with the R structure, that MgADP is bound without inducing the R→PR transition. They suggest that the crystal structure

corresponds to the weakly-bound ADP state in the myosin cycle,[6] and that the essential element in stabilizing the PR state is a change in the position of switch I to permit it to interact with $Mg^{+}2$ bound to ATP. In addition, the binding of MgATP to the rigor structure (but, apparently, not MgADP) requires motion of the P loop. The motion of Switch I is then transmitted to the cleft and the converter. Because the repositioning of Switch I appears to require times that are beyond the reach of conventional MD, we accelerate the transition by applying RTMD forces to the atoms that comprise Switch 1, MgATP, and the adjacent HG and HH helices. We were able to observe significant rearrangements in the motor domain consistent with the R→PR transition. The sequence of the observed structural changes can be summarized as follows. The movement of Switch 1 is transmitted through the adjacent HG/HH helices to the HO helix via interactions betwen nonpolar residues of the U50 subdomain (see Fig. 5). Switch 1 gradually moves away from Switch 2. The cleft hydrogen bonds K405/D570 and K405/D569 between the HO helix and Strut, and K246/Q639 between the U50 domain and the HW helix are broken and the actin-binding cleft opens. The hydrogen bond F441/A684 breaks, and the SH1 helix begins to slide along the Relay helix in the direction of the converter domain. The motion of the SH1 helix along the Relay serves to uncouple the converter from the N-terminal domain of the motor. The hydrogen bond D570/Q639 in the cleft, between the Strut and the HW helix, is broken. Full opening of the cleft is achieved after the breaking of the hydrogen bonds between residues R219[Switch 1] and E442[Switch 2].

Based on the results of simulations 2 and 3 we proposed a coupling pathway between the actin-binding cleft and the F441N/A684O hydrogen bond (OP 11), which would provide communication between the cleft and the converter. The coupling is mediated via the HR and HW helices, and the N-terminal end of the Relay. On the one hand, an intact OP 11 link between Switch 2 and SH1 helix (along with the R219/E442 salt bridge), restricts the Relay to the R position i.e. farther away from the cleft (since Switch 2 is attached to the N-terminus of the Relay), allowing the cleft hydrogen bonds K246[HO]/Q639[HW] (OP 4) and D570[strut]/Q639[HW] (OP 5) to be intact. On the other hand, a closed cleft restricts the position of the HW helix via the two hydrogen bonds (OP 4 and 5), displacing it toward the Relay (Fig. 11). The HW helix keeps the adjacent Relay helix slightly bent (in the R conformation), allowing Switch 2 to remain close enough to the SH1 helix to maintain the OP 11 bond. This hypothesis is consistent with the correlation between OP 6 [outer cleft], 10 [Relay motion], and 11 [Switch 2/SH1 helix link] (Fig. 6b–d,g–i), since it predicts that (1) breaking of OP 11 link would make the actin-binding cleft more likely to be open, or conversely, (2) opening the cleft would destabilize the OP 11 link. Furthermore, it would explain how the the OP 11 link stabilizes the closed-cleft conformation of myosin V, in which the cleft is more tightly closed than in any other myosin structure.[5]

The primary purpose of this study was to investigate mechanical coupling in myosin V, and to determine the initial events that can trigger the R → PR transition. While the scenario for the transition described above is probably close to the actual sequence of events, we note that the structures in the RTMD simulations do not correspond to a path of minimum free energy; e.g. the results of simulation 2e demonstrate that switching off the RTMD forces at the end of simulation 2, and running for 8 additional nanoseconds, leads to a partial reversal of the structural changes. In addition, the R→PS transition is not quite complete in the present simulations. Fig. 6 shows that not all final OP values for RTMD simulations 3 (as well as 2) reach values that correspond to the PR state; the differences are more significant for simulation 2, in which the actin-binding cleft does not open fully. A large discrepancy between the simulation 2 & 3 structures and the target PR structure involves the position the converter domain. Only ≃20% of the R→PR converter motion is observed in the simulations (Fig. 9). It is possible that either additional residues have to be forced to drive the R structure to a stable conformation close to the PR structure, or (and) that the duration of the present RTMD simulations needs to be extended. Consistent with this hypothesis, inclusion of Switch 2 in the

forcing set of simulation 3 leads to a simulation structure with greater resemblance to the post-rigor structure.

The simulation results are consistent with the experimental observations of negative coupling between ATP binding and actin binding,[7, 8] since in the true rigor state myosin V is bound to actin with the cleft closed. Furthermore, on the basis of X-ray structures, it was suggested that in the post-rigor conformation of myosin V, subdomains are coupled more loosely than in the rigor conformation.[6] The simulations capture the the initial stage of converter uncoupling in the R → PR transition, in which the N-terminus of the converter is repositioned by the relative motion of the Relay and SH1 helices.

To investigate the extent to which the proposed coupling pathways may be applicable to myosins in general, we aligned 38 myosin sequences from 14 myosin classes (see Supplementary Materials). Of the six residues that make sidechain hydrogen bonds in the actin-binding cleft (OP 1 – 5; res. K569 is excluded because the H-bond K569/K405 [OP 3] involves the backbone oxygen of K569), residues K246, K405, and D570 are conserved in 34, 34, and 36 of 38 sequences, respectively. Residue E566 is conserved in 18 sequences; in addition, in 10 cases Asp substitutes for E566; in the remaining 20 cases, E566 is substituted for by Gln, Met, Thr, His or Asn. These results suggest that some of the five hydrogen bonds inside the actin-binding cleft of the rigor MV are not present in other myosins, which may explain why the cleft in rigor-like MV is closed more fully than in other myosin structures. Three other structures of rigor myosin have been solved recently, two structures of MII[24] and one structure of MVI.[1] In the MVI rigor structure, only the 426K/600D interaction appears to be present, although the distance between the donor and acceptor atoms is quite large (≃ 4.5Å). The width of the outer cleft is ≃10Å vs. 7.2Å of MV. [24] In the squid MII, Q639 is changed to Val.; three of the hydrogen bonds (OP 1–5) are present, and the width of the outer cleft is 7.8Å. This structure is closest to the MV rigor structure in terms of the width of the actin-binding cleft.

Of the hydrophobic residues involved in the coupling between helices HG, HH, and HO (see Fig. 5) 40% were conserved, but nearly all substitutions preserved the hydrophobic character of the residues (e.g. by substitution of V/F/L for I; I for L, etc.). This finding suggests that the helices HG, HH, and HO are coupled in all myosins, and the communication pathway between the NBP and the cleft described in this study, which involves these helices, is likely to be universal. In addition, residue F449 that is proposed to facilitate the coupled motion of the Relay and HW helices was conserved in 33 cases, and substituted for by Leucine in the remaining five cases.

As mentioned before, the F441N/A684O H-bond is absent in all solved Xray structures of myosins except for the rigor MV structure, in which it may stabilize the closed actin-binding cleft. Although this H-bond involves only backbone atoms, introduction of a ‘bulkier’ sidechain in place of Ala at position 684 may lower the stability of the F441N/A684O bond via repulsive interactions with switch II (see Fig. 9) and Supplementary Materials). The sequence alignment indicates that in 10 of the 38 cases Ala is switched to Tyr, and in 19 cases, to Cys. In four of the five MII sequences examined it is unchanged.

Based on the present simulation results and in light of the sequence alignment analysis, we suggest the following mutagenesis studies to validate the coupling pathways proposed. To assess the role of the hydrogen bonds on the stability of the closed-cleft Rigor structure, which could impact the stability of the actomyosin rigor complex, and, indirectly, the degree of the processivity of MV, res. Q639, N398, and E566 can be mutated to those with nonpolar sidechains (e.g. Leu). The role of the F441/A684 H-bond can be studies by substituting a bulky Tyr in place of A684, which would probably result in steric hindrance that would make the F441/A684 less likely to be formed. In addition, the nearby residues Q680 and R677, which,

in the rigor structure form H-bonds with the conserved residue E164, possibly stabilizing the F441/A684 link (see Supplementary Materials), may be mutated to nonpolar residues. The resulting mutant could explain whether this H-bond, unique to MV, contributes to the high processivity of MV dimers. It would also be interesting to study the effects of the F449L (or F449V) mutation. In the present analysis, F449 facilitates communication between the actin cleft and the converter via the Relay helix. Thus, it would be interesting to know whether e.g. a smaller residue could effectively decouple closure/opening of the cleft from locking/unlocking of the converter via motion of the Relay helix and Switch II. Based on the sequence analysis, and distance from the NBP, the mutants suggested above are not expected to interfere with the hyrdolysis reaction, and could be employed in motility studies. The proposed mutations are summarized in a Table in the Supplementary Materials.

We close this section with a comparison of the present simulation results to the Normal Mode Analysis (NMA) study of Cecchini et al.[10] The normal modes (NM) are eigenvectors of the Hessian of the potential energy calculated at a local minimum. An important feature of NMA is that NM that correspond to low-frequency involve 'slow' displacements that are beyond the reach of conventional MD simulations. Cecchini et al.[10] constructed a pathway for the R→PR transition was by superposing the 40 lowest NM according to their involvement coefficients.[28] Although a small number of low-frequency NM dominate concerted large-scale motions of essentially 'rigid' subdomains, higher-frequency NM are required to account for subdomain flexibility. By using 40 NM, Cecchini et al. achieved a target (PR-like) structure with a C_α RMSD of only 1.28Å from the true PR structure. From their NM superposition model, Cecchini et al. suggested that the trigger for the R→PR transition is the interaction between switch 1 and the P-loop, which is stabilized by MgATP in the PR state. The RTMD method makes it possible to test such hypotheses by applying a localized force and monitoring the structural rearrangements induced during the MD trajectory. Moreover, while NMA does not explicitly account for thermal fluctuations and employs an implicit solvation model, RTMD simulations are done at a finite temperature and in explicit solvent.

Cecchini et al. found that the opening of the actin-binding cleft is coupled to the closing of the NBP. The present simulations confirm this finding, and show that the closing of the NBP is, in fact, the triggering event. Specifically, the displacement of Switch 1 and the adjoining helices HG/HH "pull" on the HO helix, which, in turn, stretches several hydrogen bonds within the cleft. Cecchini et al. also suggest that the breaking of the F441/A684 hydrogen bond (OP 11) decouples the converter from the motor, although, in their model, the 'sliding' of the SH1 helix between the Relay and the N-terminal domain is not directly involved in the release of the converter.

The RTMD simulations support the importance of OP 11, and suggest that converter decoupling is initiated by a displacement of the SH1 helix relative the Relay helix, which repositions the base of the converter relative to the N-terminal domain.

Cecchini et al. observed a coupling pathway between the converter and the L50 domain. Specifically, in the interpretation of the NMSM model, translation of the converter promotes a large-amplitude rotation of the L50 subdomain that leads to the complete opening of the U50/L50 cleft. In the present simulations the final positions of the converter in simulations 2 & 3 are similar, and relatively close to the starting (R) position. Thus, although using the forcing set of simulation 3 leads to complete opening of the actin-binding cleft, it does not induce the correct displacement of the converter. The mechanism for the latter is not evident from the RTMD simulations, nor is the origin of the motion of switch 2 that accompanies the opening of the cleft. Cecchini et al. proposed a tight coupling of the N-terminal subdomain to the converter through hydrogen bonds between residues 76–81 (N-term) and residues 700, 754, & 757 in the converter. In the present equilibrium NVE simulations of the rigor conformer, these

interactions were lost after ~14ns (data not shown), and thus appear too weak to produce by themselves the allosteric communication between the converter and the rest of the motor. A possible way to address this question in future simulations is to apply forces on the converter, while monitoring the state of the cleft.

Coureux et al. proposed that the communication between the NBP and the cleft in the R→PR transition involves the untwisting of a seven-tranded β-sheet located between the N-terminal and U50 subdomains. We did not see any significant untwisting of this domain in the RTMD simulations. Thus, the present results support the conclusion of Cecchini et al. that the β-sheet plays a passive role in the transition. However, since the untwisting of a β-sheet is unfavorable energetically, it may require longer time scales than simulated in this study.

Given the substantial differences between the NMA and RTMD methods, the broad agreement between the RTMD results and the findings of Cecchini et al. is encouraging, and indicates the robustness of the combined analysis. While the RTMD method described herein is limited by relatively short simulation times since explicit solvent is employed, it has shown directly how small-scale motions, such as the rupture of hydrogen bonds, couple to large-scale subdomain motions. We expect the RTMD methodology employed in this work to be be useful more generally in studies of mechanical coupling in macromolecules.

4. Materials and Methods

4.1. Preparation of structures

Crystal structures of chicken myosin V in the rigor and post-rigor conformations were obtained from the Protein Data Bank (entries 1OE9 and 1W7J, respectively). The resolution of the respective structures was 2.05Å and 2.0Å. The structures include residues 1–792 of the myosin heavy chain (HC) and the essential light chain (LC). The LC was included in all simulations since its C-terminal domain interacts with the converter of the HC. In addition, 333 and 525 water molecules that were present in the crystals of the rigor and post-rigor structures, respectively, were kept. The majority of residues of loop 2, numbered 593 to 634, were not resolved in the crystal structure. Several shorter loops, with six residues or fewer, were also not resolved. In addition, several residues had partially unresolved sidechains. The missing coordinates were provided by M. Cecchini (personal communication) from the structures generated for a normal mode analysis of the rigor and post-rigor myosin V conformers.[10] These loops are unlikely to play an important role in the simulations performed in this work; i.e. the fact that their positions are undetermined in both structures reflects their high flexibility, so that they are not expected to contribute significantly to the mechanical coupling between subdomains. For instance, loop 2 is involved in the binding to actin;[9, 15] it is very flexible and is mostly undefined in all known myosin structures. For each structure, the positions of nitrogen and oxygen atoms in the amide side groups of several asparagine and glutamine residues were switched to optimize the local hydrogen bonding patterns. Assignment of histidine protonation states was based on visual inspection of the local environment for each histidine residue. Several histidine residues were rotated about the C_β–C_γ bond to optimize the local hydrogen bonding pattern. In addition, several planar groups (e.g. phenylalanine rings) were rotated by 180° around the appropriate bond in the post-rigor structure to match the atom numbering in the rigor structure. These structural modifications are summarized in the Supplementary Materials. The post-rigor structure was crystallized with the MgATP analog MgADP·BeF_x. The ATP molecule was constructed by replacing the beryllium atom with a phosphate atom, and the fluoride atoms with oxygens. Bonds and angles involving the placed atoms were subsequently optimized by energy minimization, as described below.

The all-atom CHARMM27 topology and parameter files were used in the simulations. Water molecules present in the crystal structures were represented using the TIP3P water model.

Protons were added using the CHARMM HBUILD utility.[16] The atoms with positions known from the PDB file (called "crystal atoms" below), which included water oxygens, were fixed, and the atoms comprising the modeled loops were harmonically restrained to their modeled positions with the force constant equal to 30 kcal/mol/Å^2. The structures were minimized using the ABNR minimizer in CHARMM for 600 iterations, while the harmonic force constant on the modeled loops was reduced to 0 kcal/mol/Å^2. The crystal atoms were then harmonically restrained to their original positions, and an additional 600 cycles of ABNR minimization were performed. During this step, the force constant on the crystal atoms was gradually reduced from 5 to 0.5 kcal/mol/Å^2, and the modeled loops were not restrained. After this set of minimizations, the heavy-atom RMSD from the original PDB structures was 0.5Å and 0.43Å for the rigor and post-rigor structures, respectively.

To simulate the conformational transition of the NBP from the nucleotide-free rigor state to the post-rigor state, we first modeled a MgATP complex into the rigor structure. It would have been possible to steer the NBP from the rigor into the post-rigor conformation with the MgATP absent. However, the presence of MgATP in the NBP transition makes the process more physically realistic, since bound ATP is required for this transition to occur.[7] The coordinates for the MgATP were generated using the rigor-like myosin structure with weakly-bound ADP (PDB ID 1W7I, resolution 3.0Å) as the template. The weakly-bound ADP structure overlaps with the nucleotide-free rigor structure with an all-atom RMSD value of 0.89Å, and the NBPs of the two structures overlap with an all-atom RMSD of 0.84Å. Most of the difference comes from a slight shift in the position of the P-loop, which adjusts to coordinate the ADP molecule in the weakly-bound ADP structure. Prior to the insertion of ADP into the rigor structure, the rigor and the ADP-bound template structures were aligned by an RMSD best fit based on the NBP. The ADP coordinates were copied into the rigor structure, water molecules with any atoms within 2.0Å of the ADP were deleted, and 100 cycles of ABNR minimization were performed with 5 kcal/mol/Å^2 harmonic restraints on the crystal atoms and the newly-placed ADP molecule. Coordinates for the MgATP molecule were built by aligning the ADP moieties in the rigor and post-rigor structures and copying the Mg^{+2} ion and the γ-phosphate moiety from the post-rigor structure into the rigor structure. The residue S218 in Switch 1 is not in a position to coordinate the Mg^{+2} ion in the rigor structure; one TIP3P water molecule was added to the NBP to maintain hexacoordination of Mg^{+2}. The modeling of ATP resulted in the net loss of three water molecules from the rigor structure. The final rigor-ATP structure was then subjected to 100 cycles of ABNR minimization with harmonic restraints on the crystal atoms and the ATP, while the harmonic force constant was gradually reduced from 5 to 1 kcal/mol/Å^2. The resultant coordination of the Mg^{+2} ion in the rigor structure is shown in the Supplementary Materials.

The minimized rigor and post-rigor structures were placed in pre-equilibrated orthorhombic boxes of TIP3P water molecules. The dimensions of the boxes were 157×87×83Å^3 and 162×92×82Å^3 for the rigor and post-rigor structures, respectively. Each box had a layer of water molecules with a thickness of 10Å on each side of the protein in each dimension. Water molecules with oxygens within 2.8Å of a protein atom were deleted. This resulted in 30693 and 33416 water molecules for the rigor and post-rigor structures, respectively (in addition to the 330 and 525 water molecules that were present in the original rigor and post-rigor crystal structures). Solvation of the post-rigor structure required more water molecules than the rigor structure because the lever arm is somewhat more extended in this conformation. At this stage, the net charge of the system was $-1e$.

A small subset of water molecules was chosen randomly out of the water molecules farther away than 5Å from the protein, and replaced with K^+ and Cl^- ions. 42 K^+ ions and 41 Cl^- ions were introduced into the rigor structure, and 45 K^+ ions and 44 Cl^- ions were introduced into the post-rigor structure. The added ions neutralized the system and resulted in an approximate

ionic concentration of 150 mM. During the 1.2ns equilibration period, ions and water molecules underwent RMSD of 30Å and 40Å, respectively, and the average minimum interionic distance near the end of the equilibration was approximately 4Å for the K^+/Cl^- ion pair and 6.5Å for the K^+/K^+ and Cl^-/Cl^- ion pairs; the movement of ions during the equilibrium NVE simulations is discussed in the Supplementary Materials, where we also compare the random ion placement procedure with a method that calculates ion positions based on the electrostatic potential of the protein. The total number of atoms in the solvated systems, including hydrogens, was 108202 and 116944 for the rigor and post-rigor conformers, respectively.

All of the described coordinate manipulation steps were carried out with the CHARMM program.[17] MD simulations were performed with the NAMD program.[18] NAMD was chosen because of its favorable scaling of ≃ 70% for up to 256 processors inside a Beowulf cluster with Infiniband fabric. The following simulation parameters were used. Short-range nonbonded interactions were switched to zero between 10 and 12Å. For each atom, a neighbor-atom list was generated every 10 steps. This list included atoms that were less than 14.5Å away from the given atom. Atoms in the neighbor list were used to calculate van der Waals and short-range electrostatic interactions. Long-range electrostatic interactions were treated using Particle Mesh Ewald (PME) summation.[19] The Ewald coefficient β was 0.26, interpolation was fourth-order, and the PME grid spacing was approximately 1.0Å in each direction.

The solvated and neutralized structures were minimized with the conjugate gradient minimizer in NAMD. First, the crystal atoms (see above) and MgATP atoms were fixed, and the heavy protein atoms that were undefined in the crystal structures were harmonically restrained to their modeled positions. Added water molecules and ions were free to move. The harmonic force constant was reduced gradually from 50 to 0 kcal/mol/$Å^2$ over 600 minimization steps.

Next, crystal atoms and MgATP atoms were harmonically restrained to their initial positions with a force constant of 10 kcal/mol/$Å^2$. The structures were heated to 298K in the NPT ensemble over 100 ps. Temperature control was achieved with the Langevin Dynamics thermostat, using the BBK integrator,[20] with the friction constant set to $2ps^{-1}$, and pressure was controlled with the Langevin Piston method.[21] Both algorithms are implemented in NAMD.[18] The Langevin Piston oscillation period was 100fs and the damping period was 50fs. The pressure was maintained at 1 bar, and the simulation timestep was 1fs. Harmonic restraints were gradually reduced to zero over 1ns in the NPT ensemble, and the system was simulated without restraints for an additional 200ps. A running average of the pressure over the 200ps period for the post-rigor conformer is shown in the Supplementary Materials.

In this final step, all bonds involving hydrogens were constrained with SHAKE[22] and a timestep of 2fs was used. During the NPT equilibration step, the size of the periodic box changed from 157×87×83$Å^3$ to 154×85×81$Å^3$ for the rigor structure, and from 162×92×82$Å^3$ to 158×90×80$Å^3$ for the post-rigor structure.

After 200ps of free equilibration, the backbone-atom RMSD of the resulting structures from the respective crystal structures was 1.16 and 0.97Å for the rigor and post-rigor conformers, respectively. These structures were used as the starting point for the equilibrium MD and RTMD simulations.

4.2. Equilibrium NVE simulations

Molecular Dynamics simulations were performed in the NVE ensemble starting from the structures equilibrated in the NPT ensemble. Although all ensembles are equivalent in the thermodynamic limit, the microcanonical ensemble was chosen because it gives a more faithful description of the dynamics, i.e. although the stochastic forces due to the Langevin thermostat do not affect the equilibrium properties of the system, they introduce a decorrelation of

velocities (dependent on the Langevin friction parameter). In addition, the microcanonical ensemble requires less time per step to simulate. Simulations of 18ns were performed for both the rigor and post-rigor conformers. During the NVE simulation of the post-rigor conformer, the temperature fluctuated around 297K, with a negligible increase over the entire simulation trajectory. A plot of temperature evolution in one NVE and one RTMD simulation is provided in the Supplementary Materials.

The backbone-atom RMSD of the simulated myosin motor domains from the crystal structures remained around 1.6Å and 1.7Å for the rigor and post-rigor conformers, respectively. This value was approximately 3.0Å for both structures, if the alignment included the converter, the lever arm, and the LC. This increase in the RMSD value is not surprising, since the converter and lever arm are coupled loosely to the rest of the motor, and are thus expected to be highly flexible.[6] Root-mean-square fluctuations (RMSF) were computed from the temperature factors in the PDB files and compared to those obtained from simulation. This comparison is discussed in section §2.1.

4.3. RTMD simulations

The restrained Targeted Molecular Dynamics (RTMD) method was implemented in NAMD using the Tcl interface. The method is similar to the one already existing in NAMD, but considerably more flexible. A detailed comparison of the method with traditional Targeted Molecular Dynamics (TMD)[11] and Restricted-Perturbation (RP) TMD[23] will be presented elsewhere (Ovchinnikov & Karplus, *in preparation*). In the present approach, forces are applied on a set of atoms in one structure to control the best-fit RMSD between this structure and another (target) structure. The driving forces are computed as

$$F_{RTMD,r_i} = -k(RMSD(\hat{r},\hat{r}_T) - \delta) \times \frac{\alpha_i(r_i - r_{T,i})}{RMSD(\hat{r},\hat{r}_T)} \quad (1)$$

$$\alpha_i = min\{1, \frac{\Delta r_{max}}{\left\| r - r_T \right\|}\} \quad (2)$$

In the above equations, N is the number of atoms to which forces are applied, k is the force constant, r_i is the i-component of the atomic position of the atom located at r, $\hat{r}$ and $\hat{r}_T$ represent the current and target structures, respectively, δ is decreased linearly in time from the initial RMSD value between the two sets of atoms included in the restraints to a final value (taken as 0.1Å in the simulations), and F_{RTMD,r_i} is the i-component of the force on the atom located at r. With Eq. 1 and 2, no atom experiences a force greater than the force which would be applied if the distance between its current and target positions, denoted r and r_T, respectively, were Δr_{max}. It can be seen from Eq. 2 that when the simulation structure is sufficiently close to the target structure (in the sense that for each atom, the distance between the current and target positions is less than Δr_{max}) the forces can be expressed using the (RTMD) potential

$$E_{RTMD} = \frac{Nk}{2}(RMSD(\hat{r},\hat{r}_T) - \delta)^2 \quad (3)$$

as

$$F_{RTMD,r_i} = -\frac{\partial E_{RTMD}}{\partial r_i} = -k(RMSD(\hat{r},\hat{r}_T) - \delta)\frac{(r_i - r_{T,i})}{RMSD(\hat{r},\hat{r}_T)} \quad (4)$$

In the present RTMD simulations, the force constant was set to 0.1 kcal/mol/Å^2, and the value for the cutoff was Δr_{max}=5Å. The value for the force constant was chosen such that the final simulation value for $RMSD(\hat{r}, \hat{r}_T)$ was around 1.25Å. A similar value would be expected for the RMSD of an equilibrated MD structure from the initial crystal structure. Although it is possible to reduce this value by employing a larger force constant, this is undesirable for two reasons. First, increasing the force constant would likely cause the structure to deviate more from the equilibrium (i.e. the path of minimum free energy) during the transition. Second, once the value of $(RMSD(\hat{r}, \hat{r}_T) - \delta)$ reaches $\simeq$ 1.0Å, the RTMD forces would mostly act to suppress the amplitude of thermal fluctuations of the forced atoms, rather than cause further conformational change. The value of Δr_{max} was chosen to lead to approximately equal forces on all atoms in the forcing set in the early stage ($\simeq$ 100ps) of the RTMD simulations. We note that for the simulations performed in this work, the choice of Δr_{max} is probably not significant because the the forcing sets (described in the §2.3) are quite small, and the transition of the forcing sets between the initial and target structures is relatively simple. Thus, the likelihood of biasing the sequence of events in the transition is small. The magnitudes of the RTMD forces applied to the forcing sets are discussed in the Supplementary Materials.

In the present RTMD simulations, the set of atoms used for best-fit RMSD orientation was different from the set of atoms to which forces are applied. This approach is especially useful for pairs of structures in which one or more domains are in very similar conformations. One can then overlay the structures based on these domains while forcing other domains into their positions in the target structure. When the sets of orientation atoms and forced atoms are not the same, a net force and torque act on the system. Consequently, additional forces have to be applied to keep the system from translating and rotating in the simulation box. Fifty-two (52) backbone atoms of the alpha helix HF, comprised of residues 170–182, were restrained to their original positions with harmonic potentials of the form $\frac{k}{2}\left\|r_i - r_i^0\right\|^2$, where r_i denotes the position of atom i, and the superscript 0 refers to the initial position. The force constant k was set to 0.5 kcal/mol/Å^2. These restraints should have no effect on the transition path because the best-fit RMSD between the helix backbone in the two conformations is only 0.23Å. Consequently, the HF helix is expected not to be involved in the conformational change, and to remain intact during the transition. Partitioning of the simulation structure into the orientation and forcing sets employed in a representative RTMD simulation is illustrated in the Supplementary Materials.

Three forcing sets were studied; they are discussed in §2.3.

The RTMD simulations are conducted in the NVT ensemble with the temperature set to 298K using Langevin Dynamics as the thermostat. The simulation time step was 2fs. A Langevin friction coefficient of 2ps^{-1} was used for temperature control. It is desirable to keep this coefficient low to minimize dissipative work that is performed on the system by RTMD forces, and to avoid slowing down the rate of structural changes. The evolution of the temperature in a representative RTMD simulation (see Supplementary Materials) indicates that satisfactory temperature control is achieved with this low value of the friction coefficient. In particular, comparison with the evolution of the temperature in an NVE simulation, indicates that the fluctuations in the instantaneous temperature are of similar magnitudes in the two cases.

Supplementary Material

Refer to Web version on PubMed Central for supplementary material.

Acknowledgments

The authors thank Marco Cecchini for a careful reading of the manuscript and for many comments that improved the final version. MK and VO thank Anne Houdusse for discussions concerning myosin V. The authors acknowledge partial financial support by a grant from the Human Frontiers Grant Science Program. VO and BLT acknowledge partial financial support from the Singapore-MIT Alliance. The work done Harvard was supported in part by a grant from the National Institutes of Health. VO acknowledges partial financial support under the NRSA fellowship 1F32GM083422-01. VO and MK are grateful to NERSC for providing supercomputer resources for several calculations performed in this study. Supplementary information accompanying this article can be accessed on-line.

References

1. Yildiz A, Forkey JN, McKinney SA, Ha T, Goldman YE, Selvin PR. Myosin V walks hand-over-hand: single fluorophore imaging with 1.5 nm localization. Science 2003;300:2061–2065. [PubMed: 12791999]
2. Rief M, Rock RS, Mehta AD, Mooseker MS, Cheney RE, Spudich JA. Myosin-V stepping kinetics: a molecular model for processivity. Proc Natl Acad Sci USA 2000;97:9482–9486. [PubMed: 10944217]
3. Huxley HE. The mechanism of muscular contraction. Science 1969;164:1356–1359. [PubMed: 4181952]
4. Holmes KC, Schroder RR, Sweeney HL, Houdusse A. The structure of the rigor complex & its implications for the power stroke. Phil Trans R Soc B 2004;359:1819–1828. [PubMed: 15647158]
5. Coureux PD, Wells AL, Menetrey J, Yengo CM, Morris CA, Sweeney HL, Houdusse A. A structural state of the myosin V motor without bound nucleotide. Nature 2003;425:419–423. [PubMed: 14508494]
6. Coureux PD, Sweeney HL, Houdusse A. Three myosin V structures delineate essential features of chemo-mechanical transduction. EMBO J 2004;23:4527–4537. [PubMed: 15510214]
7. De La Cruz EM, Wells AL, Rosenfeld SS, Ostap EM, Sweeney HL. The kinetic mechanism of myosin V. Proc Natl Acad Sci USA 1999;96:13726–13731. [PubMed: 10570140]
8. Holmes KC, Angert I, Kull FJ, Jahn W, Schroder RR. Electron cryo-microscopy shows how strong binding of myosin to actin releases nucleotide. Nature 2003;425:423–427. [PubMed: 14508495]
9. Volkmann N, Liu H, Hazelwood L, Krementsova EB, Lowey S, Trybus KM, Hanein D. The Structural Basis of Myosin V Processive Movement as Revealed by Electron Cryomicroscopy. Mol Cell 2005;19:595–605. [PubMed: 16137617]
10. Cecchini M, Houdusse A, Karplus M. Allosteric Communication in Myosin V: From Small Conformational Changes to Large Directed Movements. PLoS Comput Biol 2008;4:e1000129. [PubMed: 18704171]
11. Schlitter J, Engels M, Kruger P, Jacoby E, Wollmer A. Targeted molecular dynamics simulation of conformational change – Application to the T→R transtion in insulin. Mol Sim 1993;10:291–308.
12. Li G, Cui Q. Mechanochemical Coupling in Myosin: A Theoretical Analysis with Molecular Dynamics and Combined QM/MM Reaction Path Calculations. J Chem Phys 2004;108:3342.
13. Koppole S, Smith JC, Fischer S. The Structural Coupling between ATPase Activation and Recovery Stroke in the Myosin II Motor. Structure 2007;15:825–837. [PubMed: 17637343]
14. Yu H, Ma L, Yang Y, Cui Q. Mechanochemical Coupling in the Myosin Motor Domain. II Analysis of Critical Residues. PLoS Comput Biol 2007;3:0214–0230.
1. Menetrey J, Bahloul A, Wells AL, Yengo CM, Morris CA, Sweeney HL, Houdusse A. The structure of the myosin VI motor reveals the mechanism of directionality reversal. Nature 2005;435:779–785. [PubMed: 15944696]
15. Murphy CT, Spudich AS. The Sequence of the Myosin 50–20K Loop Affects Myosin's Affinity for Actin throughout the Actin–Myosin ATPase Cycle and Its Maximum ATPase Activity. Biochemistry 1999;38:3785–3792. [PubMed: 10090768]

16. Brünger A, Karplus M. Polar hydrogen positions in proteins: empirical energy placement and neutron diffraction comparison. Proteins: Struct Funct Genet 1988;4:148–156. [PubMed: 3227015]
17. Brooks BR, Bruccoleri RE, Olafson BD, States DJ, Swaminathan S, Karplus M. CHARMM: A Program for Macromolecular Energy, Minimization, and Dynamics Calculations. J Comput Chem 1983;4:187–217.
18. Phillips JC, Braun R, Wang W, Gumbart J, Tajkhorshid E, Villa E, Chipot C, Skeel RD, Kale L, Schulten K. Scalable Molecular Dynamics with NAMD. J Comput Chem 2005;26:1781–1802. [PubMed: 16222654]
19. Essmann U, Perera L, Berkowitz ML, Darden T, Lee H, Pedersen LG. A smooth particle mesh Ewald method. J Chem Phys 1995;103:8577–8593.
20. Brünger A, Brooks CB, Karplus M. Stochastic boundary conditions for molecular dynamics simulations of ST2 water. Chem Phys Lett 1984;105:495–499.
21. Feller SC, Zhang Y, Pastor RW, Brooks BRJ. Constant pressure molecular dynamics simulation: The Langevin Piston Method. J Chem Phys 1995;103:4613–4621.
22. Ryckaert J-P, Ciccotti G, Berendsen HJC. Numerical integration of the cartesian equations of motion of a system with constraints: Molecular dynamics of n-alkanes. J Comput Phys 1977;23:327–341.
23. van der Vaart A, Karplus M. Simulation of conformational transitions by the restricted pertrubation targeted molecular dynamics method. J Chem Phys 2005;122:114903. [PubMed: 15836253]
24. Yang Y, Gourinath S, Kovács M, Nyitray L, Reutzel R, Himmel D, O'Neall-Hennessey E, Reshetnikova L, Szent-Györgyi AG, Brown JH, Cohen C. Rigor-like Structures from Muscle Myosins Reveal Key Mechanical Elements in the Transduction Pathways of This Allosteric Motor. Structure 2007;15:553–564. [PubMed: 17502101]
25. Houdusse A, Kalabokis VN, Himmer D, Szent-Györgyi AG, Cohen C. Atomic Structure of Scallop Myosin Subfragment SI complexed with MgADP: A Novel Conformation of the Myosin Head. Cell 1999;97:459–470. [PubMed: 10338210]
26. Houdusse A, Sweeney HL. Myosin motors: missing structures and hidden springs. Curr Opin Struct Biol 2001;11:182–194. [PubMed: 11297926]
27. Li G, Cui Q. Analysis of Functional Motions in Brownian Molecular Machines with an Efficient Block Normal Mode Approach: Myosin-II and Ca^{2+}–ATPase. 2004
28. Ma J, Karplus M. Ligand-induced conformational changes in *ras* p21: a normal mode and energy minimization analysis. J Mol Biol 1997;274:114–131. [PubMed: 9398520]

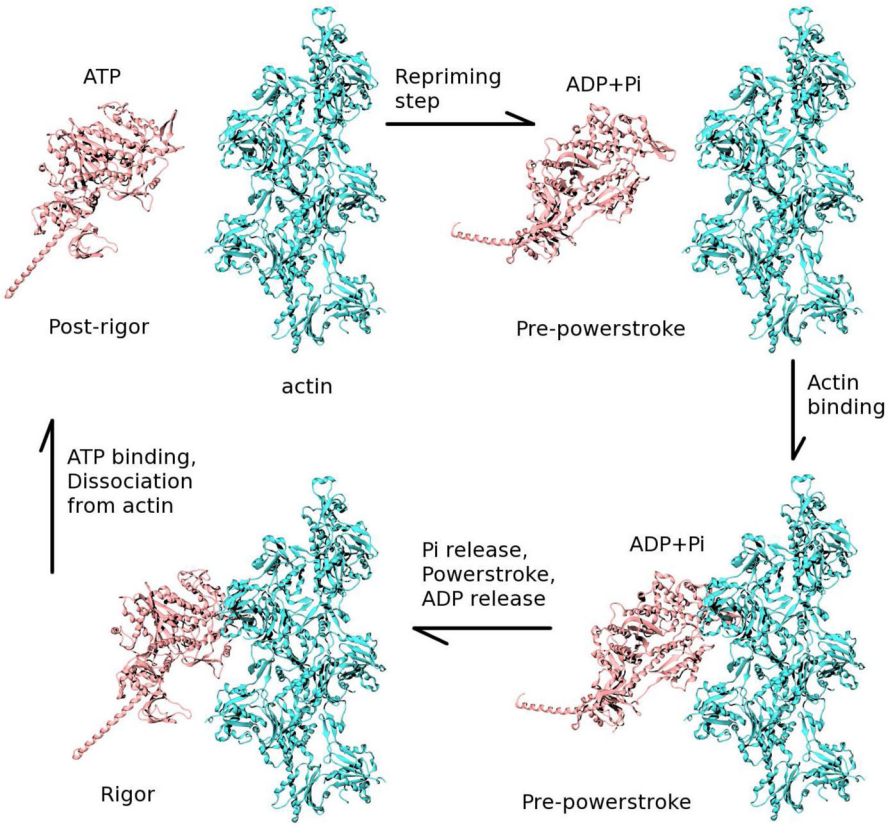

Figure 1.

A simplified description of the actomyosin cycle. For clarity, only five actin monomers are shown. The actin filament is drawn in cyan, and myosin is in pink. The coordinates of the actomyosin rigor complex were taken from the model of Holmes et al.[4] The approximate conformation of the MV PPS state was obtained by rotating the converter domain manually in accord with the MII PPS structure (e.g. Holmes et al. 2004,[4] Fig. 7a).

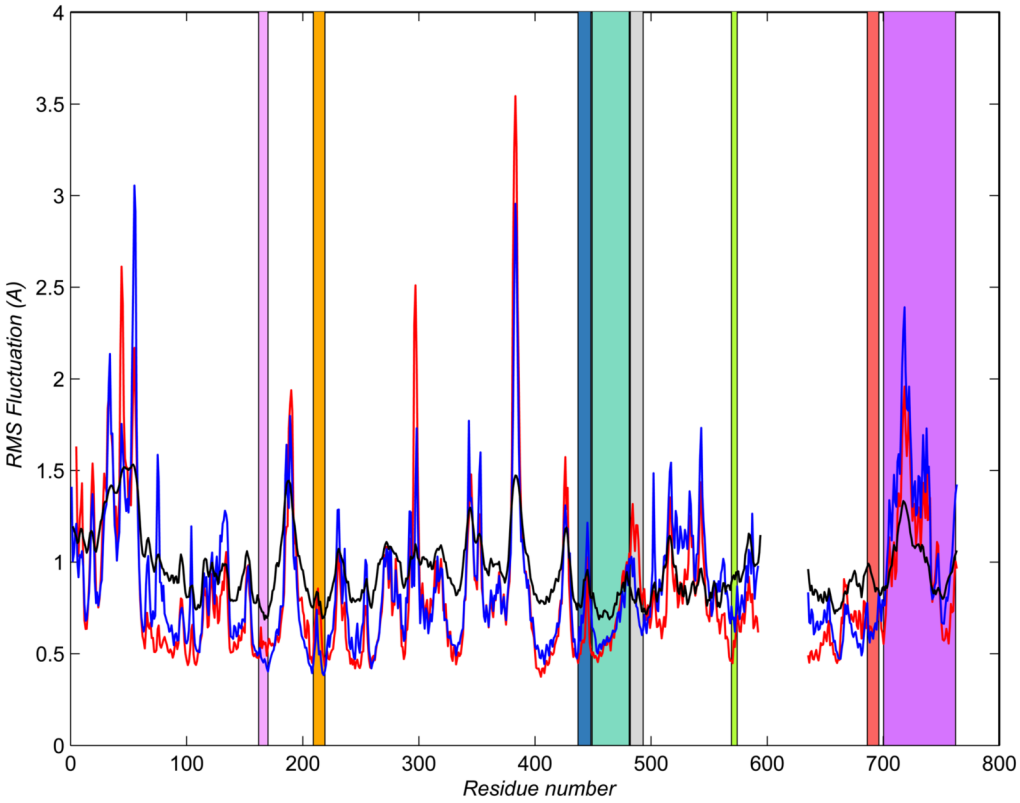

Figure 2.

Root-mean-square fluctuations (RMSF) of residues from their average positions computed from equilibrium MD simulations and from the B-factors in the post-rigor PDB file. Simulation data corresponding to residues 593–634 in loop 2, which was disordered in the crystal structures, are not shown. Each frame in a trajectory is aligned with the first frame using backbone atoms of the motor domain; red line: rigor; blue line: post-rigor conformer; black line: B-factors in the post-rigor PDB file; those for the rigor PDB file are similar. Key domains are highlighted as follows. Pink: P-loop, Orange: Switch I, Blue: Switch II, Cyan: Relay helix, Gray: Relay loop; Light green: Strut; Red: SH1 helix; Magenta: Converter.

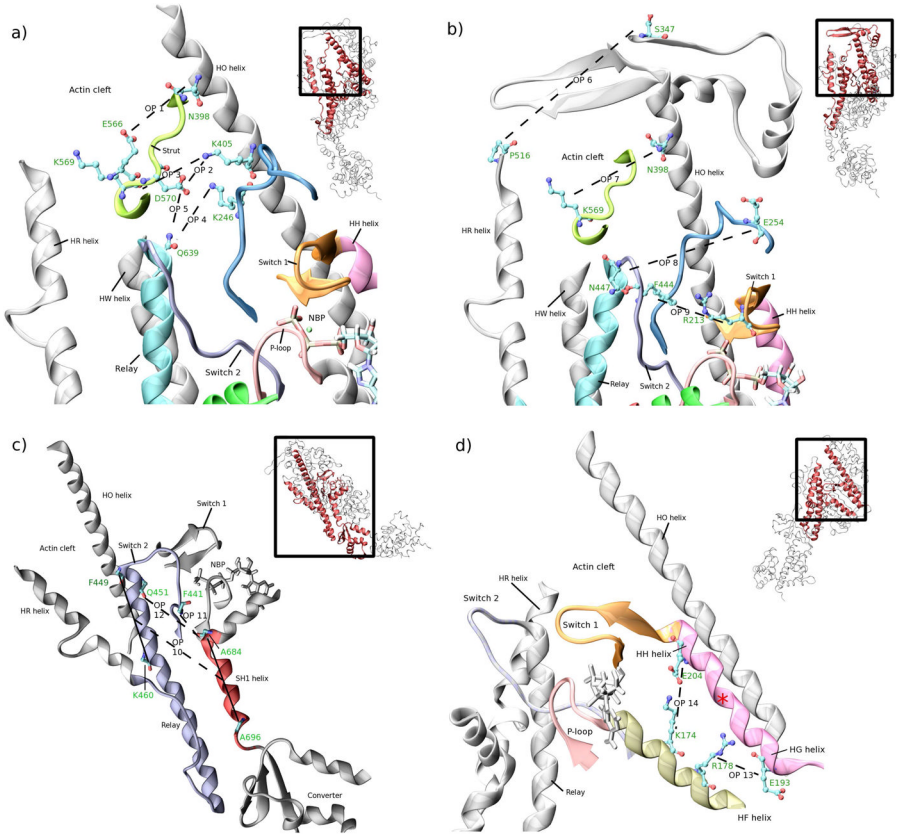

Figure 3.

Illustration of the OP listed in Tab. 2 used to characterize the rigor and post-rigor structures of myosin V. Only the post-rigor structure is shown for clarity; a) OP 1–5, b) OP 6–9, c) OP 10–12, d) OP 13–14. Although helices HG (N191–N200) and HH (P201–I206) are drawn as a single helix (pink), they are separate helical domains because of the ‘helix-breaker’ residue P201; the position of P201 is marked by a red asterisk.

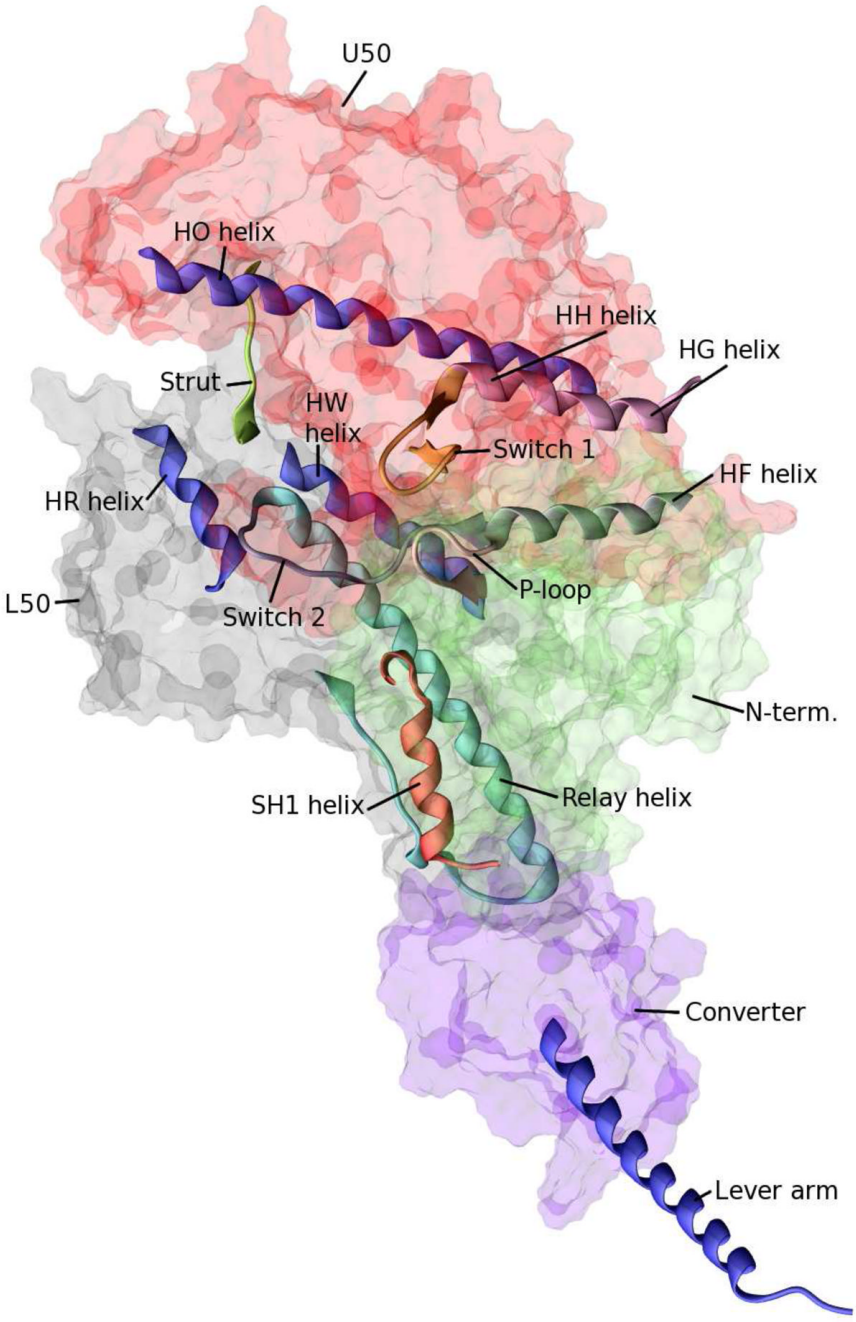

Figure 4.
Myosin V subdomains defined in Tab. 3. The Upper 50 kDa (U50), the lower 50 kDa (L50), and the N-terminal (N-term) subdomains are drawn as red, gray, and green transparent surfaces, respectively. The Essential Light Chain (ELC) is omitted.

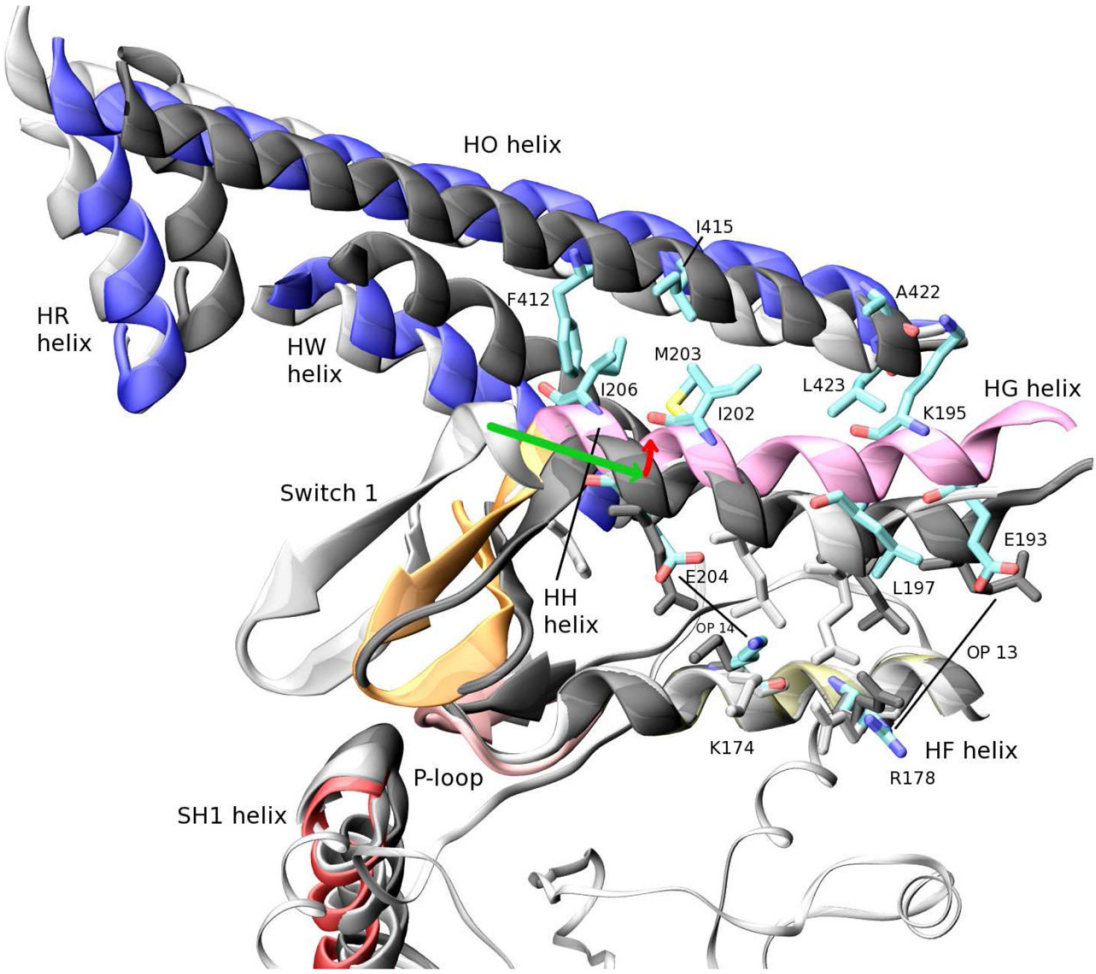

Figure 5.

RTMD simulation 1. Final simulation structure (color), initial simulation structure (light gray), and the target (PR) structure (dark gray) are superimposed on the backbone of the HF helix, which was kept stationary in the simulation. Nonpolar residues I202, M203, I206, I415, F412, and L423 that occupy the interface between helices HO, HG, and HH are shown. Nonpolar residue V196 mentioned in the text cannot be seen in this orientation. Residue pairs R178/E193 and K174/E204, which correspond to OP 13 and 14, respectively, are connected with solid lines in the PR structure. Nitrogen *NZ* of K195 forms a salt bridge to the backbone oxygen of A422. The green arrow indicates the direction of motion of the HG/HH helices from the R state to the PR state expected on the basis of the Xray structures; the red arrow indicates the direction of additional motion of these helices observed in RTMD simulation 1.

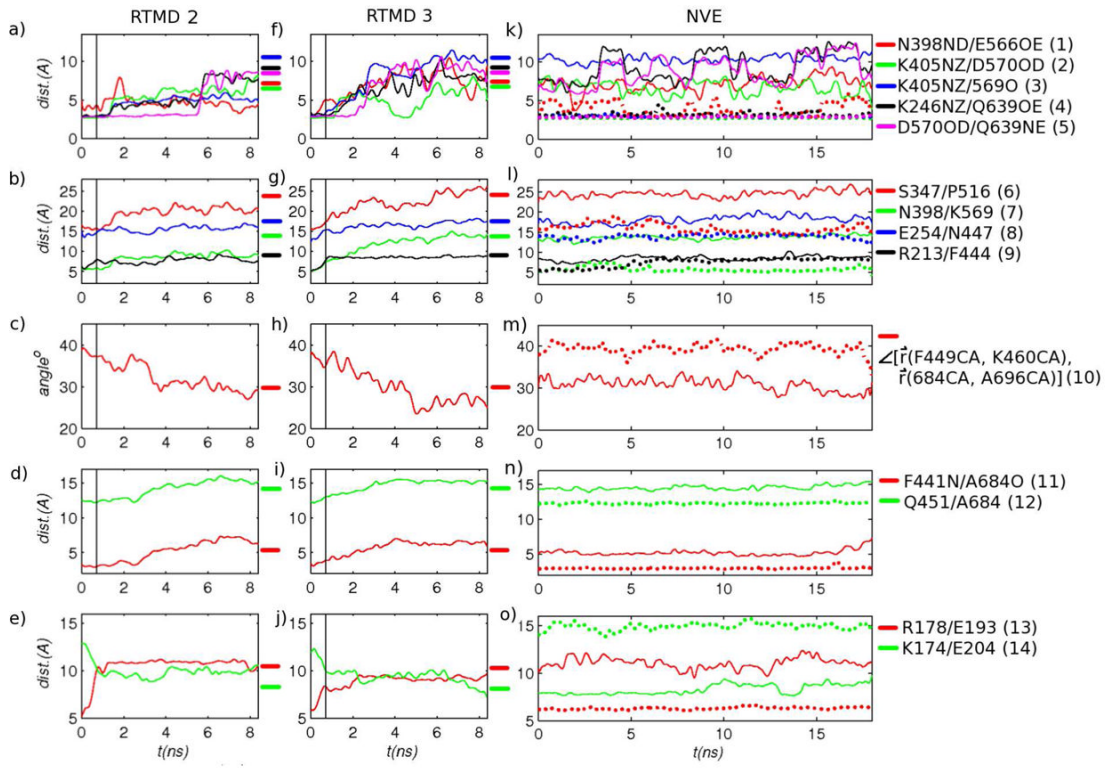

Figure 6.

Evolution of OP in RTMD simulations 2, 3, and equilibrium NVE simulations. The solid vertical line marks the time (0.7) at which $\delta = 0.1$. δ remains at this value for the remainder of the simulation; (a–e) RTMD simulation 2; (f–j) RTMD simulation 3; (k–o) NVE simulations; solid line, post-rigor NVE; dotted line, rigor NVE. To make the plots clearer, a 30ps running average is applied to each OP time series. The approximate values of the OP that correspond to the PR structure are indicated with horizontal lines to the right of subfigures a–j. In the legend entries, the numbers in parentheses correspond to the OP defined in Tab. 2.

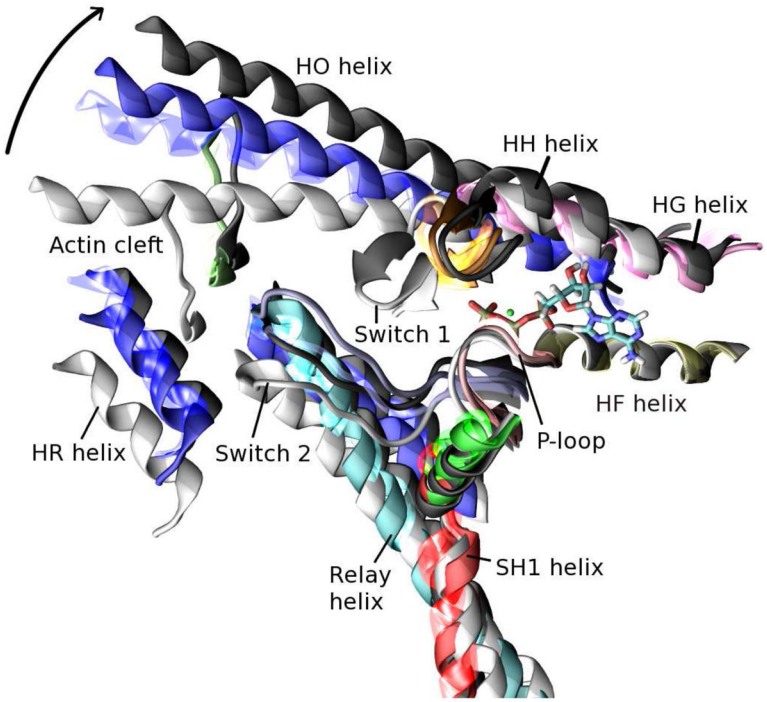

Figure 7.
Two RTMD simulation 2 structures superposed on the initial and target structures. The superposition is performed on the backbone of the HF helix. Light gray: initial (rigor) structure; transparent colors: simulation at t = 1.0; solid colors: t = 8.4, dark gray: target (post-rigor) structure. By t=1.0 the HO helix has undergone a large part of its displacement, although the actin-binding cleft has not opened (Fig. 6).

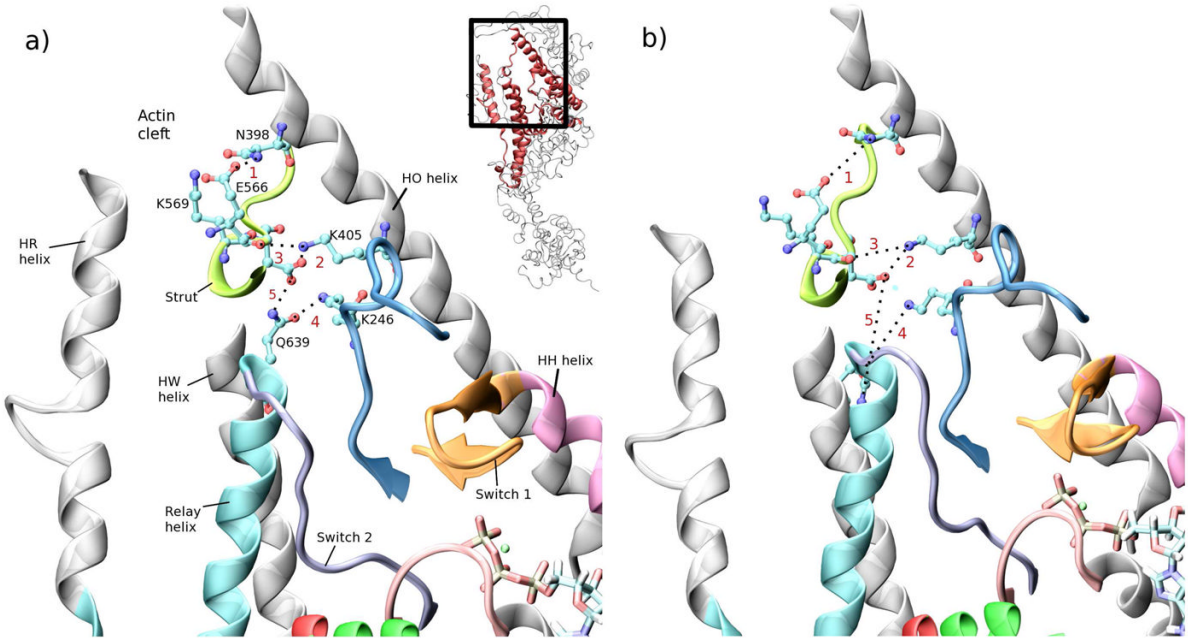

Figure 8.

Rupture of hydrogen bonds in the cleft in RTMD simulation 2; a) initial simulation structure (rigor); hydrogen bonds N398/E566, K405/D570, K405/D569, K246/E639, D570/Q639 are intact; b) final simulation structure;all five hydrogen bonds are broken (see also Fig. 6). Numbers correspond to the OP defined in Tab. 2. Hydrogen bonds are indicated by dotted lines.

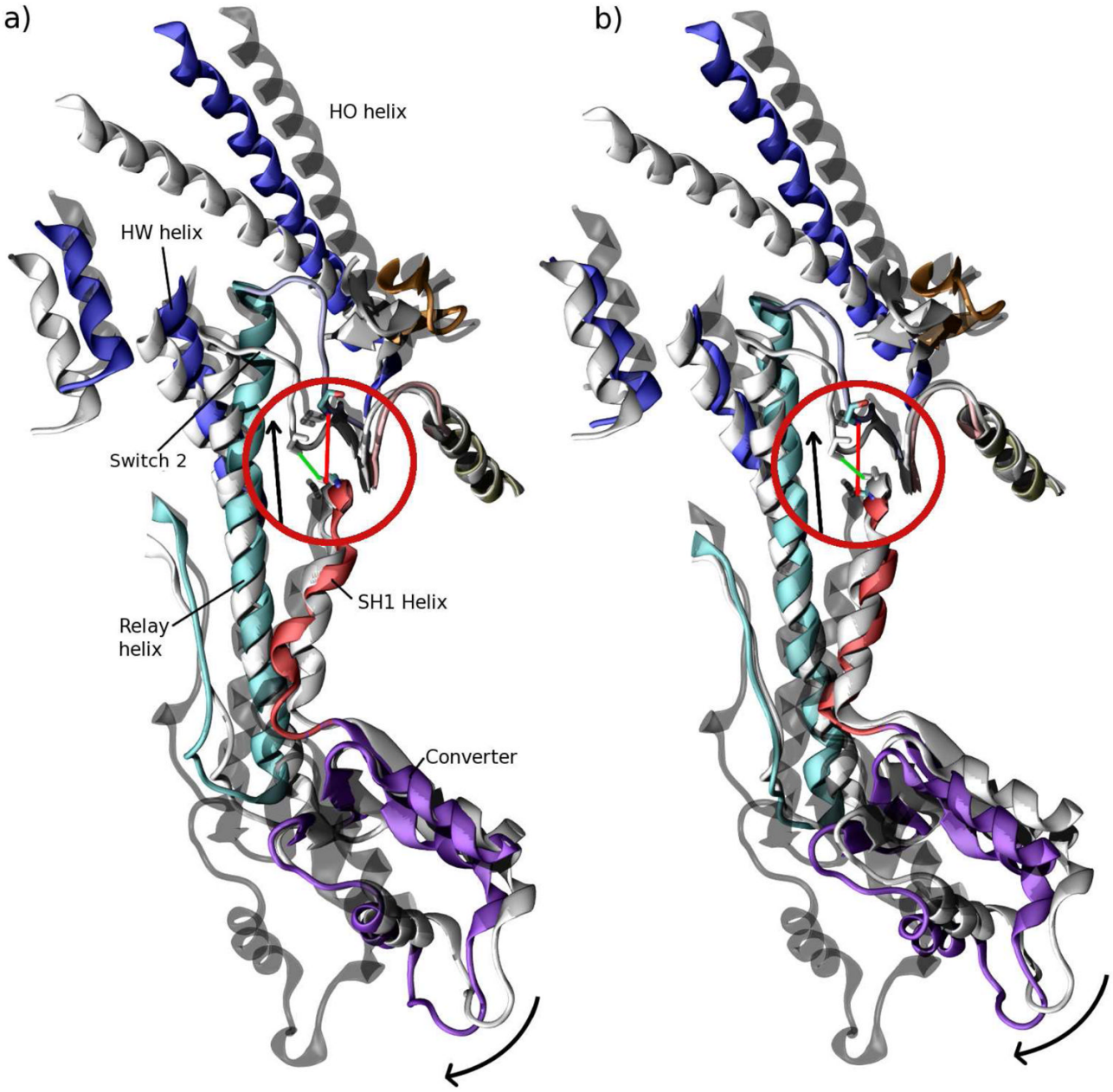

Figure 9.

Converter repositioning in RTMD simulations 2 (a) and 3 (b). Light gray: initial (R) structure; color: final simulation structure; dark gray (transparent): target (PR) structure. Straight black arrow indicates the direction of motion of the Relay helix relative to the SH1 helix. Curved arrow indicates the direction of converter displacement. The green and red lines show the F441N/A684O distance corresponding to the initial and final simulation 2 (a) and simulation 3 (b) structures, respectively.

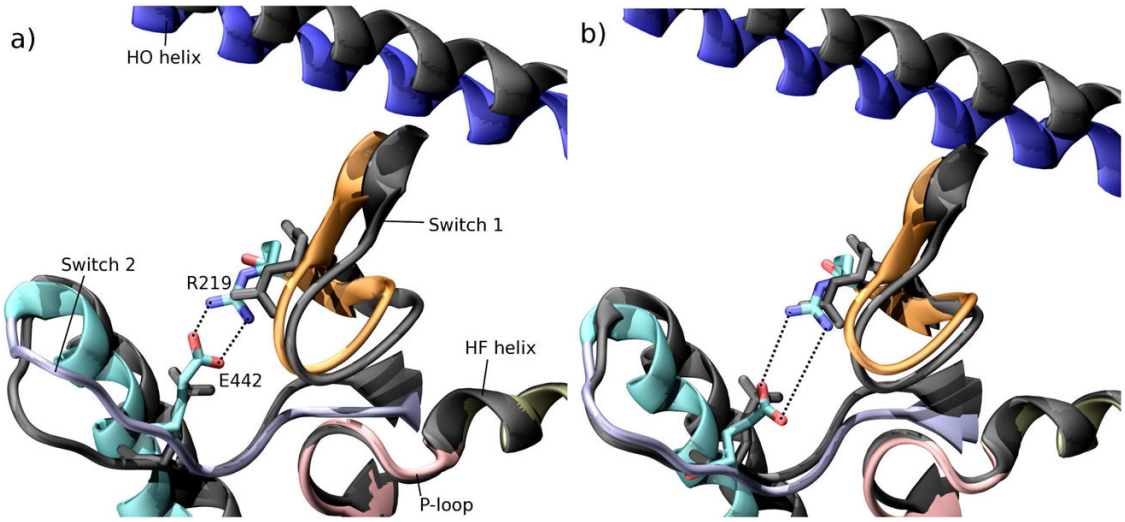

Figure 10.
Switch 2 position in simulations 2 (a) and 3 (b). Color: final simulation structure; dark gray: target structure (PR). In a) the average distance between the guanidinium nitrogens of R219 and carboxyl oxygens of E442 is 3.2Å, and in b) it is 5.9Å.

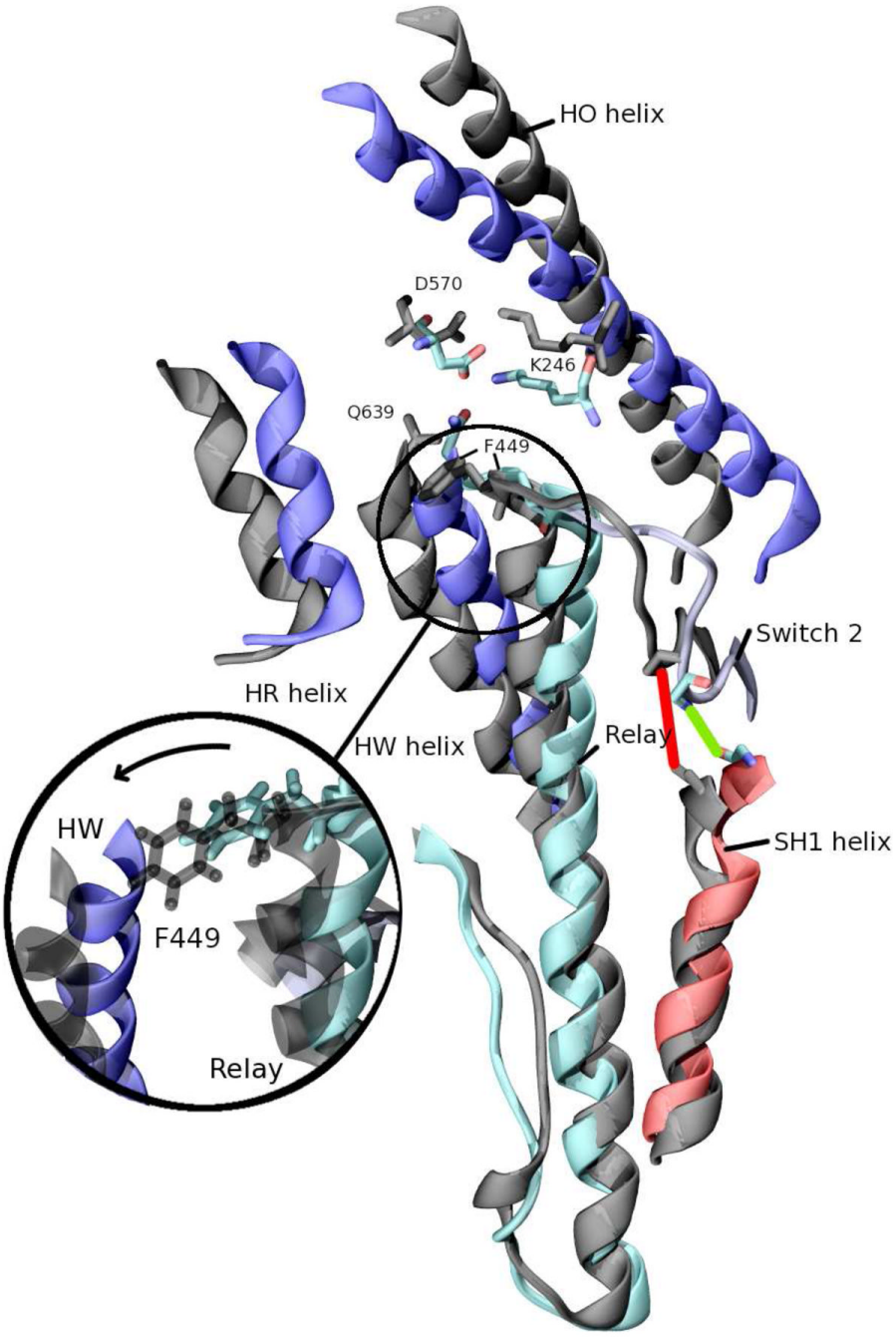

Figure 11.

Conformation of the Relay helix. Color: R structure; dark gray: PR structure; The structures are superimposed on the Relay and SH1 helices to show their orientation relative to each other. The N-terminus of the Relay helix is oriented differently in the R and PR structures, and affects the state of the cleft (see OP 10 in Tab. 2 and Fig. 3h and 6c,h Curved arrow indicates the direction of Relay displacement in the R→PR transition. The green and red lines show the F441N/A684O distance corresponding to the R and PR structures, respectively. Inset: F449 facilitates coupled motion of the HW and Relay helices.

Table 1

Summary of NVE simulations in the absence of external forces. Quoted RMSD was computed using the backbone atoms of the motor domain excluding the flexible converter domain. The corresponding residues are 1–593, 635–698 using chicken myosin V numbering.

Struc.	Total time	final RMSD from PDB structure
R	18 ns	1.6 Å
PR	18 ns	1.7 Å

Table 2

Order parameters (OP) that characterize the rigor and post-rigor states of myosin V. “COM distance” indicates that the distance was computed between the centers of mass of all of the atoms in a residue. The last and next-to-last columns show the average OP value calculated from the equilibrium NVE simulations of the post-rigor and rigor states, respectively. The OP are illustrated in Fig. 3. Their behavior during equilibrium NVE simulations is shown in Fig. 6k–o. Distances are quoted in Å, and angles are quoted in degrees.

OP#	Description	Atoms involved	Type	R val.	PR val.
1	Cleft HB	N398N_{δ}, E566O_{ε}	distance	3.89	7.11
2	Cleft HB	K405N_{ζ}, D570O_{δ}	distance	2.71	6.60
3	Cleft HB	K405N_{ζ}, K569O	distance	2.91	10.27
4	Cleft HB	K246N_{ζ}, Q639O_{ε}	distance	3.21	9.26
5	Cleft HB	D570O_{δ}, Q639N_{ε}	distance	2.85	8.81
6	Far outer cleft	S347, P516	COM distance	15.99	24.51
7	Outer cleft	N398, K569	COM distance	5.80	13.72
8	Inner cleft	E254, N447	COM distance	13.87	18.13
9	Far Inner cleft	R213, F444	COM distance	7.49	8.49
10	SH1 helix/Relay orient.	F449C_{α}, K460C_{α}, A684C_{α}, A696C_{α}	angle between $r\rightarrow$(F449C_{α},K460C_{α}) & $r\rightarrow$(A684C_{α},A696C_{α})	39.44	30.84
11	Sw.2/SH1 link	F441N, A684O	distance	3.01	5.22
12	SH1 helix/Relay orient.	Q451, A684	COM distance	12.29	14.56
13	HG helix position	R178, E193	COM distance	6.30	11.03
14	HH helix position	K174, E204	COM distance	14.90	8.28

Table 3

Subdomain definitions for myosin V (Anne Houdusse, *private comm.*). Chicken myosin V numbering is used (UniProt sequence ID Q02440). Subdomain name abbreviations that are used in the text are given in parentheses. Smaller subdomains that are part of the larger Nterm, U50, and L50 subdomains are listed below the corresponding subdomain name.

Domain name	Definition (res. ID)
N-terminal domain (N-term)	63–183, 656–683
P-loop	162–169
HF helix	170–182
Upper 50 kDa domain (U50)	201–448, 575–634
HH helix	201–206
Switch 1	207–219
HO helix	393–425
Switch 2	437–448
Lower 50 kDa domain (L50)	449–574, 635–655
HR helix	504–515
Strut	568–574
HW helix	637–652
HG helix	191–200
Relay helix	449–481
SH1 helix	686–697
Converter	699–764
Lever arm	769–795

Table 4

Summary of RTMD simulations. The simulation and reference structures were aligned based on the atoms in the orientation set. RTMD forces were applied only to the atoms that belong to the forcing set. δ_0 refers to the initial RMSD between the two conformations of the atoms in the forcing sets. The orientation set only included the positions of the backbone atoms, N, C, O, and C_α. These atoms were also harmonically restrained to their initial positions with the harmonic force constant of 0.5 kcal/mol/Å^2. The numbers in parentheses correspond to the number of atoms in the corresponding sets. The RTMD force constant was set to 0.1 kcal/mol/Å^2. The total duration of all simulations was 8.4ns. The simulation corresponding to entry 2e is a continuation of simulation 2, in which the force constant was reduced to 0 kcal/mol/Å^2 from time t=8.4 to t=9.4, and the simulation was further continued without forces until t=16.8. The final RMSD was computed using all backbone atoms in the motor domain. At the beginning of the simulations, this RMSD was approximately 3.5Å. Time is quoted in nanoseconds.

#	Direction	Orientation set	Forcing set	δ_0	time to δ = 0.1	final RMSD (Å) from target
1	R→PR	HF (52)	Switch 1, MgATP, P-loop (177)	5.10	0.5	2.45
2	R→PR	HF (52)	Switch 1, MgATP, HG, HH (252)	6.46	0.7	2.16
2e	R→PR	HF (52)	Switch 1, MgATP, HG, HH (252)	0.1		2.90
3	R→PR	HF (52)	Switch 1/2, MgATP, HG, HH (353)	5.81	0.6	1.83
4	PR→R	HF (52)	Switch 1, MgATP, HG, HH (252)	6.46	0.7	2.21